IMPEDANCE AND SIGNAL QUALITY MEASUREMENTS FOR MICROELECTRODE ARRAYS IMPLANTED CHRONICALLY IN FELINE SPINAL NERVES

by

Shubham Debnath

B.S. in Biomedical Engineering, University of Minnesota, 2011

B.S. in Mathematics, University of Minnesota, 2011

Submitted to the Graduate Faculty of

Swanson School of Engineering in partial fulfillment

of the requirements for the degree of

Master of Science

University of Pittsburgh

2013

UNIVERSITY OF PITTSBURGH

SWANSON SCHOOL OF ENGINEERING

This thesis was presented

by

Shubham Debnath

It was defended on

November 25, 2013

and approved by

Xinyan Tracy Cui, Ph.D., Associate Professor, Department of Bioengineering

Robert A. Gaunt, Ph.D., Assistant Professor, Department of Physical Medicine and Rehabilitation

Thesis Advisor: Douglas J. Weber, Ph.D., Associate Professor, Department of Bioengineering

IMPEDANCE AND SIGNAL QUALITY MEASUREMENTS FOR MICROELECTRODE ARRAYS IMPLANTED CHRONICALLY IN FELINE SPINAL NERVES

Shubham Debnath, MS

University of Pittsburgh, 2013

The spinal nerves, consisting of ventral roots and dorsal root ganglia, are a novel target for motor and sensory interfaces for neural prosthetic limbs. By implanting floating microelectrode arrays (FMA) into the spinal nerves, it is possible to record single unit activity from motor axons in the ventral roots (VR) or microstimulate sensory fibers in the dorsal roots and dorsal root ganglia (DRG). The ventral roots remain a lesser-explored electrophysiological target for motor control of a neuroprosthetic device. Long term acquisition of high quality neural recordings is necessary for neuroprosthetic applications and electrical interface impedance measurements are often used as a diagnostic tool to evaluate electrode integrity. However, it is not well understood how electrode impedance affects the quality of single unit recordings, particularly in the spinal nerves where few chronic recording studies have been performed.

This study characterizes ventral root recordings by examining signal-to-noise ratios (SNR) and single unit yield for chronically implanted microelectrode arrays in cats. Two 32-channel floating microelectrode arrays (FMA, MicroProbe, Inc.) were implanted into the L6 and L7 ventral roots of 9 cats during sterile surgery. Single unit recordings were performed during treadmill locomotion and under anesthesia. All recorded units were classified as motor or sensory by heuristic metrics after all data were manually spike sorted. For all motor-related units, SNR and single unit yield were calculated for each electrode. The SNR and yield measures were grouped by electrode site size to examine the effect of site size and electrode impedance on

recording quality. The electrode site exposures ranged from 25 to 160 μm, yielding initial impedance values in the range of 50-500 kΩ. As expected, electrode impedances were inversely correlated with site size. However, SNR and yield did not differ significantly across this wide range of electrode sizes; peaks in both probability of unit detection and median SNR values did not consistently fall within a particular range of impedances. Both SNR and yield decay over time, as expected, but all electrodes recorded spikes with SNR > 2 out to 12 weeks post-implant. Results from this study are being used to improve the design and specifications of exposed tip lengths of microelectrodes for chronic neural recording in spinal nerves.

TABLE OF CONTENTS

LIST OF TABLES

LIST OF FIGURES

PREFACE

Acknowledgements:

Sincere thanks to all members of the Rehab Neural Engineering Lab (RNEL), particularly Erin Garia for assistance with animal care, Matt Bauman for support during recording sessions, and Tyler Simpson for aid in setting up impedance measurements and other engineering-related projects.

Special thanks to my parents, Joyati and Narayan Debnath, for their constant love and guidance throughout my tenure at the University of Pittsburgh.

Funding:

This work was sponsored by the Defense Advanced Research Projects Agency (DARPA) Microsystems Technology Office under the auspices of Dr. Jack Judy (jack.judy@darpa.mil) through the Space and Naval Warfare Systems Center, Pacific Grant No. N66001-11-C-4171.

1.0 INTRODUCTION

Emerging from the growth in the field of biotechnology, neural engineering and the development of neural prosthetics have opened up the possibility of creating man-made devices that can replace lost motor and sensory function [1]. This has manifested the prospect of restoring limb function to amputees or patients suffering from paralysis [1, 2, 3]. In 2005, nearly 2 million people in the United States were living with the loss of a limb, and it is projected that this number will double by 2050 [4], due to vascular disease, trauma, and cancer. Meanwhile, in 2009, a survey showed that approximately 1.3 million people in the United States are suffering from some form of paralysis resulting from spinal cord injury [5]. These two patient populations make up just over 1% of the United States population, and both could benefit greatly from neural prosthetics. There is active research in the advancement of thought-controlled assistive devices that extract motor-related information from the central nervous system (brain and spinal cord) and translate this content into commands to control an external apparatus [1, 2, 3, 6]. The studies in this thesis summarize a way to further this research by pursuing a unique electrophysiological target, the ventral spinal roots, for motor-related recordings and examining electrode design and its influence on recorded signal quality.

1.1 NEURAL PROSTHETICS

Neural prosthetics are devices that record from or stimulate the nervous system with the purpose of improving or replacing motor, sensory, or cognitive ability that has been damaged due to disease or injury. Often, these devices interface directly with the central and/or peripheral nervous system to detect the activity of individual or groups of neurons [6]. This electrical activity can be interpreted by a computerized algorithm to manipulate an external tool or computer or, conversely, this electrical activity can be influenced by controlled stimulation.

At this time, only a few neural prostheses have had clinical and commercial success. One is deep brain stimulation (DBS) for the treatment of Parkinson's disease, tremor, dystonia, chronic pain, and major depression. DBS is implanted in over 100,000 patients worldwide, according to Medtronic, Inc. [7]. Another successful example is the cochlear implant (Figure 1.1B), which is placed in the inner ear to partially restore hearing in the profoundly deaf. Cochlear implants have been implanted in approximately 219,000 patients worldwide as of 2012, according to the National Institute of Health (NIH), allowing them to understand speech, environmental sounds, and even enjoy aspects of music [8]. A more recent development in neural prosthetics is the retinal prosthesis (Figure 1.1C), which is intended to restore functional vision in patients suffering from partial or total blindness. The first commercially available product, ARGUS II from Second Sight Medical Products, Inc., has been approved for use in Europe since 2011 and by the FDA for sale in the United States on February 14, 2013 [9].

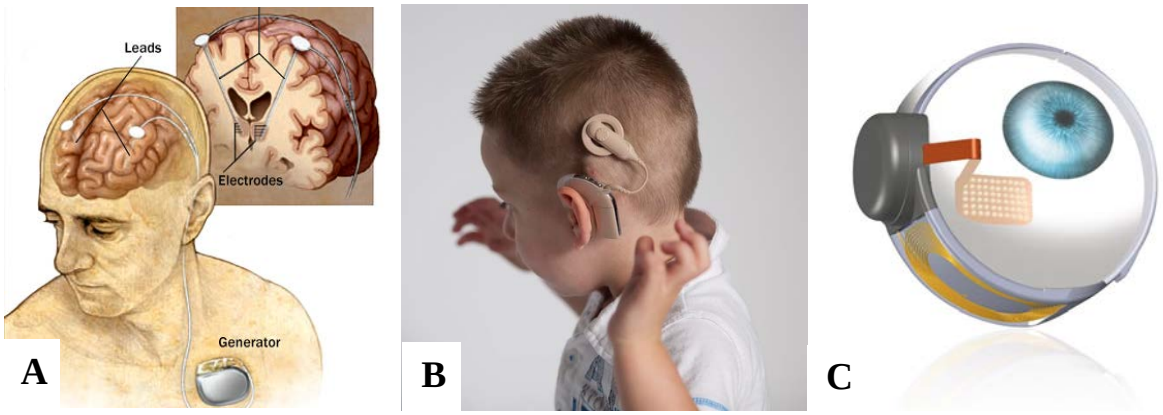

Figure 1.1. Examples of successful neural prosthetics. A. Deep Brain Stimulator, B. Cochlear Implant, C. Retinal Prosthesis (Images from Mayo Clinic, Sydney Cochlear Implant Clinic, and Discovery)

1.2 MODERN NEURAL RECORDING TECHNIQUES

Techniques to measure and record neural activity are available in a number of modalities that can be divided by surgical invasiveness and then further by size, temporal resolution, and spatial resolution (Figure 1.2).

1.2.1 Noninvasive modalities

One of the least invasive techniques is electroencephalography (EEG). EEG (Figure 1.3A) utilizes a network of large electrodes that can be applied directly to the surface of the scalp to record cortical activity through the skull and skin. EEG signals are analyzed by spectral content [10], pinpointing the type of neural oscillations observed as well as using a number of processing algorithms to localize these signals in the brain [11, 12]. EEG has a very poor spatial resolution

but has been useful for the diagnosis of sleep disorders [13, 14] and epilepsy [11, 15, 16]. EEG is quite portable, as it only requires a headcap and recording software.

Another noninvasive technique is magnetoencephalography (MEG). MEG (Figure 1.3B) records magnetic fields produced by electrical currents traveling naturally in the brain using superconducting quantum inference devices (SQUIDs), which are very sensitive magnetometers. MEG has a similar spatial resolution [17, 18] and a better temporal resolution than EEG [19, 20], but can only sense tangential components of current sources in the brain; EEG is sensitive to both tangential and radial components [19]. MEG is also not portable, requiring a magnetically shielded room and a large MEG machine; nonetheless, it has an important role in diagnostic applications [21] and the study of various cognitive processes such as vision [22], audition [23], and language processing [24].

There are other non-invasive modalities, such as functional magnetic resonance imaging (fMRI), but they have not been used prosthetic applications, which are described section 1.3.

1.2.2 Invasive modalities

Significantly more invasive than EEG or MEG, electrocorticography (ECoG) applies a flexible array of electrodes implanted under the skull and upon the surface of the brain (Figure 1.3C). Also known as intracranial EEG (iEEG), ECoG signals are composed of synchronized local field potentials (LFP) recorded from the exposed surface of the cortex. The LFP signal is produced by the summation of synaptic current flowing within a volume of neural tissue. Because of its direct contact with the brain, the spatial and temporal resolution is much higher than any noninvasive neural recording technique. The LFP picked up by surface ECoG provides a measure of a neural

population within 1 centimeter of the recording electrode, and the temporal resolution is approximately 5 milliseconds [25].

The most invasive neural recording technique is single unit recording, which apply penetrating microelectrodes implanted within the cortex (Figure 1.3D) or spinal cord. Single unit recordings have the greatest spatial and temporal resolution, capable of characterizing individual neurons by recording the change in voltage within or close to the cell membrane. The work in this thesis utilizes single unit recordings from a floating microelectrode array (FMA) implanted within the spinal roots to measure extracellular action potentials.

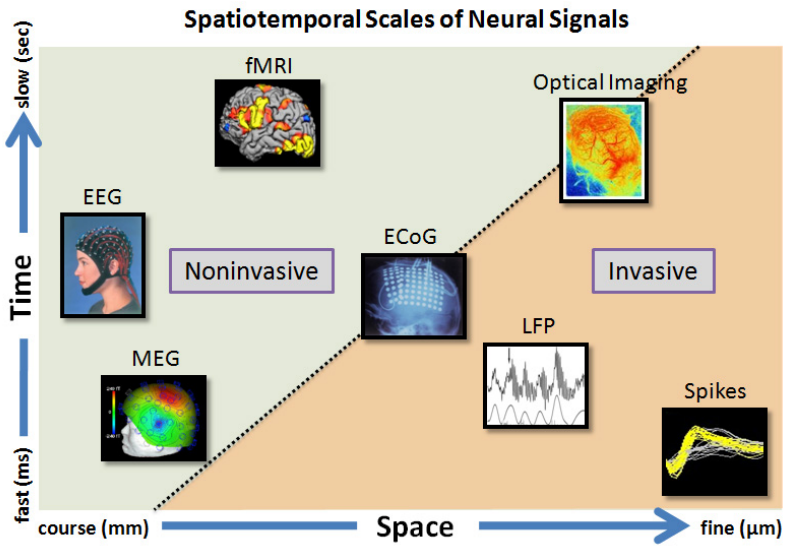

Figure 1.2. Summary of neural recording modalities. Shown above are the spatial and temporal resolutions of various recording methods, as well as invasiveness. (Image by IEEE)

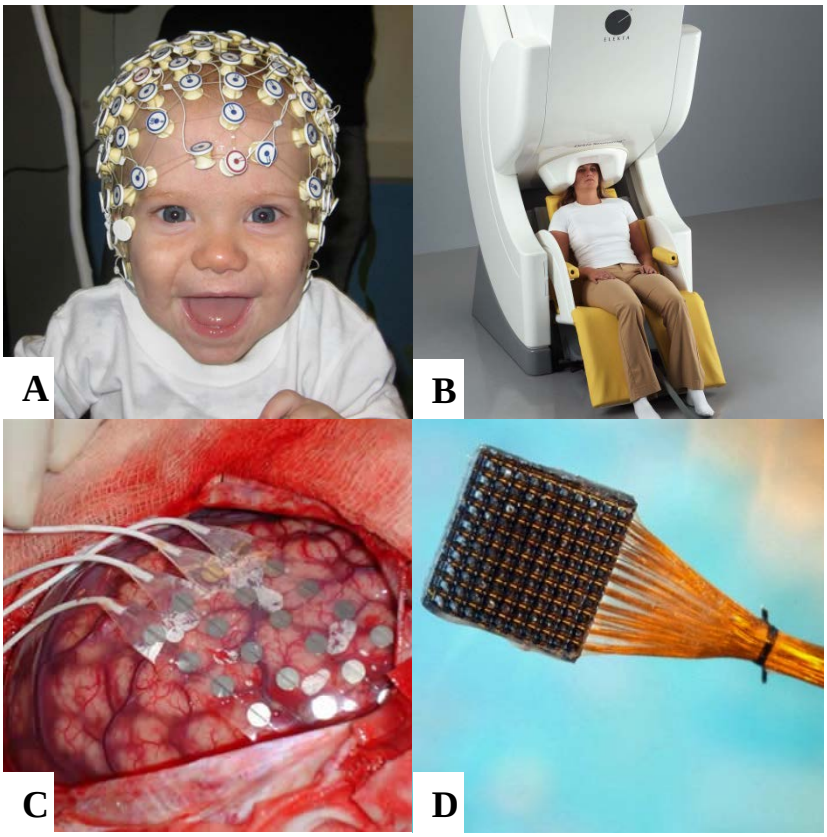

Figure 1.3. Examples of neural recording modalities. A. EEG head cap, B. MEG machine, C. ECoG array implanted on brain surface, D. Intracortical microelectrode array (Images by Boston Children's Hospital, Massachusetts Institute of Technology, and University of Utah)

1.2.3 Other electrophysiological recording techniques

Other than the brain and spinal cord (which, along with the retina, collectively make up the central nervous system), there are other targets in the human body for electrophysiological recordings, particularly the peripheral nerves. Invasive recordings from nerves can detect spike trains from efferent and afferent nerve fibers, providing a direct measure of the neural drive to the muscles and sensory feedback back to the central nervous system. There are number of

different types of electrodes designed for a peripheral nerve interface, including cuffs, flat interface nerve electrodes (FINE), and longitudinally implanted intrafascicular electrodes (LIFEs) [26]. The cuff is an extraneural device consisting of an insulating tubular sheath that completely surrounds the nerve and contains contacts that are exposed to the nerve itself [27]. The FINE is a variation of the cuff, designed to reshape peripheral nerves into a favorable geometry for more fascicular separation, and therefore more selective stimulation and recording [28]. LIFEs, on the other hand, are intrafascicular electrodes, placed within the nerve with direct contact to the tissue for stimulation or recording [29].

Electromyography (EMG) is another signal that can be used to measure motor intent by measuring electrical activity produced by the contraction of skeletal muscles. EMG signals are composed of superimposed motor unit action potentials, with size, shape, and frequency determined by the location of the electrode with respect to the muscle fibers [30]. When a muscle is at rest, EMG should not detect any spontaneous activity. As the muscle contracts, action potentials appear; with a stronger contraction, more and more muscle fibers produce action potentials at varying rates and amplitudes [30].

1.3 MOTOR PROSTHETICS

Assistive devices, known as motor prosthetics, have been developed to restore function for individuals suffering from tetraplegia and patients that are missing limbs. These devices are based on a number of recording modalities, resulting in neural control of a virtual neuroprostheses in 2D and 3D space or the movement of a robotic arm.

1.3.1 Noninvasive motor applications – Brain

EEG has been implemented in systems that allow patients to communicate by mentally spelling words on a screen [Schalk 2004] or controlling a cursor in 2D or 3D space [31, 32, 33]. EEG has also been used to control a virtual arm in real-time; users were able to control the end-point (fingertip) of a virtual arm from a center position to one of four peripheral targets [34]. Furthermore, control of a virtual hand was achieved by matching given hand grasps by decoding field potentials collected by EEG [35].

MEG has been used as rehabilitation therapy for individuals with paralysis. It has been demonstrated that MEG could be used to allow individuals with chronic and complete hand paralysis to control a computer cursor and hand orthosis by modulated sensorimotor rhythms [35]. Participants in the study were able to complete a brain-machine interface (BMI) controlled grasping task. Using visual, tactile, and proprioceptive feedback of an orthosis could improve task performance further and promote plasticity in rehabilitation applications. Visual feedback using virtual reality models are useful for neurofeedback and will be used in the future for most MEG (and EEG) studies for noninvasive methods [36].

1.3.2 Invasive motor applications – Brain

Arm movement is well represented in activity recorded from groups of neurons in the motor cortex. Cortical signals have been used to control a multi-jointed prosthetic device with direct real-time interaction with the physical environment. Non-human primates were implanted with intracortical microelectrode arrays in their primary motor cortices; the monkeys used signals

from the arrays to control a robotic arm to feed themselves [37] (Figure 1.4A). This study was a demonstration of the ability of using recording from a cortical microelectrode array to control a multi degree-of-freedom prosthetic, while paving the way towards the development of more complex prosthetic devices that could achieve natural arm and hand function [1, 37, 38]. However, it can be noted that these cortical neural prostheses are not acceptable for clinical use, as they must retain the ability to reliably record from large populations of neural for long periods of time, ideally the length of a human lifetime. Microelectrode implantations are currently restricted to research settings [2]. In a research study in 2013, two 96-channel intracortical microelectrodes were implanted in the motor cortex of an individual with tetraplegia [39]. The patient was able to move the prosthetic limb freely in a three-dimensional workspace by the second day of training, and a variety of movement tasks could be performed routinely by the end of 13 weeks of brain-machine interface training.

However, ECoG has been used in human studies as recently as this year (Figure 1.4B). An ECoG-based system was implanted into a human participant with tetraplegia caused by a high level (C4) spinal cord injury [40]. By recording ECoG signals with a high density 32-electrode grid over the hand and arm area sensorimotor cortex, the participant was able to achieve robust control of a robotic arm in three dimensions, finding success in a number of arm movement and hand grasp tasks over the implantation period of 28 days.

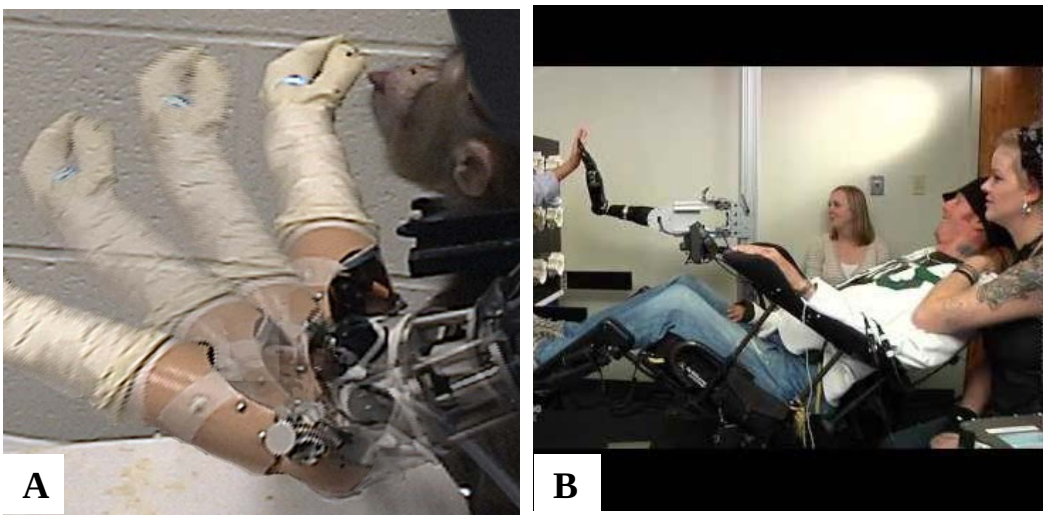

Figure 1.4. Examples of control of upper limb neuroprosthetics. A. Monkey feeding using robotic arm controlled by recordings from cortical microelectrode array, B. Human using robotic arm controlled by ECoG recordings (Images from University of Pittsburgh)

1.3.3 Other examples of motor control

The peripheral nerves have also been the target for recording neural activity for the control of a motor prosthetic device [41]. Four LIFEs were implanted in the median and ulnar nerves of an amputee and they provided output signals for 4 weeks. These signal patterns were used to control multiple hand grasps executed by a robotic hand. It can be noted that sensory feedback was also successfully delivered via the LIFEs for the first 10 days of the implant [41].

Myoelectrically controlled prostheses rely on muscle contractions as a signal to activate motor prostheses [Micera 2010]. They function by detecting a signal via surface EMG electrodes which then control electric motors. First developed in 1960 by the Central Prosthetic Research Institute of the USSR [42], myoelectric prostheses are among the most distributed clinical hand

prosthetics for amputees; patients can manipulate a simple hand grasp by contraction of a targeted residual muscle group. Not all upper extremity amputees benefit from use, and over 80% of patients discard their prosthesis [43]. The EMG signal is compared to a fixed threshold; by overcoming this threshold, on/off signals are procured and used to control the opening and closing of a hand [26].

Myoelectric control has also been improved by the adaptation of Targeted Muscle Reinnervation (TMR) [44]. TMR is more invasive, as it requires a surgery that transfers multiple residual nerves into a target muscle region. Once reinnervated, these target muscles, usually in the chest or upper arm, serve as biological amplifiers of motor commands from the transferred arm nerves [44]. After the surgery, surface EMG signals can be measured to control prosthetic arms [45]. In one study, it was found that TMR patients were able to control two degrees-of-freedom with an experimental upper limb prosthetic [46]. Later on, it was shown that the patients were able to repeatedly perform 10 different motions at the elbow, wrist, and hand with a virtual prosthetic arm [44].

While many of the described motor prosthetics can be viewed as successful, there remain disadvantages to each one. EEG and MEG lack the spatial and temporal resolution, and portability in MEG's case, for signals to smoothly and appropriately be translated into movement of a natural robotic prosthetic. Using depth microelectrodes and ECoG in the brain requires highly invasive surgery and a craniotomy, and can generate inflammatory responses due to trauma and foreign body tissue response. Peripheral nerve implants (nerve cuff, LIFE) also require invasive surgery; they are not immune to EMG noise and contain mixed motor and sensory signals. Myoelectric devices (aside from surface EMG), including TMR, require invasive surgeries, leading to a long recovery time, and they are not single unit capable. All of

these considerations lead to the call for examining further areas for motor-related activity. The spinal roots, specifically the ventral root, are lesser-explored targets that contain motor units and can be accessed using a microelectrode.

Table 1.1. Comparing key features of various peripheral nerve interface technologies. Green, red, and yellow dashes signify 'yes', 'no', and 'uncertain', as shown in the legend.

Legend: Yes / No / Uncertain — Feature	Device: Myoelectric	TMR	Nerve Cuff	Intrafascicular Life-Like	Intrafascicular Microelectrode	Regenerative	Ventral Root
High SNR							
Single Unit Capable							
Highly Scalable							
Reduced Susceptibility to EMG Noise							
Stationary Environment							
Mechanically Protected Environment							
Compatible with Brachial Plexus Injuries							
Immune to Afferent Neural Activity							
Isolated Motor & Sensory Signals							
Minimally Invasive Implant							
Demonstrated recordings > 1 month							
High Bandwidth							
High Dynamic Range							
Human Ready Devices							

1.4 TARGETING VENTRAL ROOTS

Table 1.1 describes usability and performance features of a variety of peripheral nerve interface methods. By targeting the spinal roots with floating microelectrode arrays (FMA), it is possible to record single units. Because of the unique organization of the spinal roots (Figure 1.5), it is possible to independently access pure motor signal in the ventral roots; sensory signals are

segregated and can be found in the corresponding dorsal root ganglia. The location in the spine allows mechanical protection and isolation from any EMG interference, as the vertebral bones surround the nerve. The ventral root approach is highly scalable by using high-density arrays, while high bandwidth and dynamic range recording is feasible. It is highly important to note that the ventral root approach is the only direct nerve interface that may be able to be clinically established without open surgery, eliminating surgical morbidity and reducing system cost. There are well-established minimally invasive clinical procedures for accessing the cervical spinal nerves [47], which can be applied for spinal root electrode implants in the future.

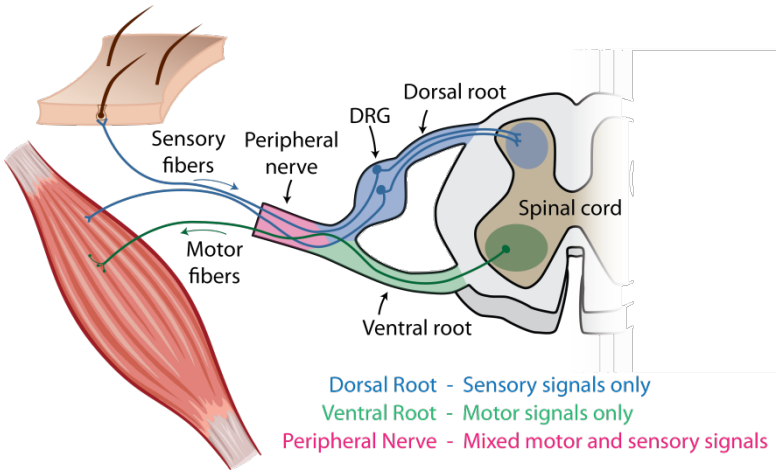

Figure 1.5. Diagram of the anatomy of the spinal roots. The ventral root, in green, contain only motor signals, while dorsal root and dorsal root ganglia (where neuronal cell bodies exist) only contain sensory signals. The signals mix in the peripheral nerves (in pink).

Andy Hoffer, Jerry Loeb, and colleagues provided initial feasibility for ventral root recordings over 25 years ago [48, 49, 50, 51]. They performed chronic recordings in cats using flexible wire microelectrodes; up to 12 ‘hatpin’ microelectrodes were inserted in the fifth lumbar

(L5) ventral root. While allowing the cats to move freely, individual units could be recorded for a whole day or longer, allowing recording to occur during a range of activities and over long period of time. The studies also found that the modulation of firing frequency closely resembled modulation in EMG amplitude recorded in leg muscles. Motor unit recordings were made in ventral root axons over several months, but the chronic stability of these recordings was never characterized. By applying modern commercially available technology, the floating microelectrode array (FMA, MicroProbe, Inc), the studies in this thesis test and characterize ventral root recordings based on signal-to-noise ratios and unit yield over time, as well as refine electrode design by measuring electrical impedances of variety of exposed tip sizes and analyzing any relationships with signal quality.

1.5 THESIS ORGANIZATION

This thesis studies ways to characterize neural recordings from the ventral root over time, as well as apply electrical impedance measurements to predict signal quality. Chapter 1 described current neural prothestics and studies of motor control by a number of neural recording modalities, as well as further motivation and reasons for targeting the ventral root. Chapter 2 dicusses the framework of the methods used for analysis and principles of neural recording. The novel analysis of the neural recordings is also established in Chapter 2, along with background on electrical impedance measurement and past work relating it to neural signals. In Chapter 3, the signal quality of chronic ventral root recordings are quantified; the implant surgery and experimental methods are explained in detail with results summarized by subject and by array. In Chapter 4, the electrical impedance experiments are reviewed, with impedance measurements

related to signal quality; further site size analysis and future steps in electrode design are considered. Chapter 5 summarizes the conclusions of previous chapters and their impact to the future of neural engineering.

2.0 BACKGROUND OF METHODS

This study focuses on the interpretation of single unit recordings and the quantification of signal stability by analyzing signal-to-noise ratios and unit yield, along with examining electrode durability and design. To achieve these, a comprehension of the basics of electrical recording and impedance studies is necessary.

2.1 PRINCIPLES FOR NEURAL RECORDING

When a metal electrode is placed inside a physiological medium, an interface is formed. Within this interface, charge must be transduced from electrolytes in the physiological medium to an electric current in the metal at the recording site or contact. The electrochemical reactions that occur at the interface are described in great depth in Merrill et al. [52] and Cogan [53]. As electrons move from the electrolyte to electrode, there is a change in electrical potential at the electrode/electrolyte interface, producing an electric field [52].

One common strategy for neural recording involves the use of an electrode to measure the local voltage at a recording site, which can convey information about the spiking activity of one or more nearby neurons [54]. The firing of a single neuron is characterized by a

stereotypically shaped signal known as an action potential. Action potentials are often recorded with microelectrodes implanted in close proximity to target neurons [53].

The objective of single unit neural recording is to measure action potentials from single neurons with a high signal-to-noise-ratio for extended periods of time. While several studies have shown reliable recordings using microelectrode arrays in rats, monkeys, and humans on the order of a few years [2, 55, 56, 57, 58, 59], ventral root signals have not been thoroughly analyzed since the Hoffer-Loeb studies in the 1980s.

2.1.1 Separating Motor and Sensory Signals

Because of the unique anatomy of the spinal roots, when targeting motor units with penetrating microelectrodes, it is important to ensure that neural signals are being recorded from the motor-related ventral root, as opposed to the sensory-related dorsal root ganglia; while motor and sensory signals are segregated within the spinal roots, electrode tip lengths and orientations can vary, potentially resulting in misplaced electrodes ending up in the dorsal root.

For this study, an algorithm was developed to classify signals as sensory or motor. After spikes were hand sorted for each recorded channel (described more in section 3.2.4), each separated unit was analyzed individually, using a number of heuristic metrics that allowed classification as motor or sensory. These metrics included the maximum inter-spike interval, the response to passive movement during anesthesia, and classification of other units recorded from the same electrode.

The inter-spike interval (ISI) refers to the time between two successive spikes in a spike train. After setting a threshold for a maximum ISI (~100 milliseconds to focus on fast time

dynamics of the firing rate), a sum of two Gamma distributions was fit to the ISI histogram. Two distributions were used to discern high firing rate ‘doublets’ from the primary mode of the firing rate. Dynamic movements can induce very brief motor unit ISIs (2-5 milliseconds) known as ‘doublets’ [60], which are different from the usually spaced discharges (at least 20 milliseconds) seen with muscle contraction [61]. After model fitting, separation between the two Gamma distributions was tested. If there is no separation between the Gamma distributions by measuring the overlap of area under the curves, the peak was checked to be greater than 20 milliseconds. If there is considerable separation, the second (later) and larger peak must be at greater than 20 milliseconds for a unit to be classified as motor activity. If the Gammas distributions peak occured at less than 20 milliseconds, the unit was classified as sensory.

After statistical testing, two other checks were done. First, if the same channel was active during an anesthetized trial on the same day (when there should be no spontaneous motor activity), it was not classified as a motor unit. Second, units on the same channel were checked; because there is only one contact site per electrode shaft, it is unlikely that motor and sensory units would be recorded on the same channel. If the channel has confirmed motor units, it is likely that other units on the channel are also motor units. By these methods, each separated unit went through three independent tests to verify motor-related activity. The flowchart in Figure 2.1 describes the classification methods.

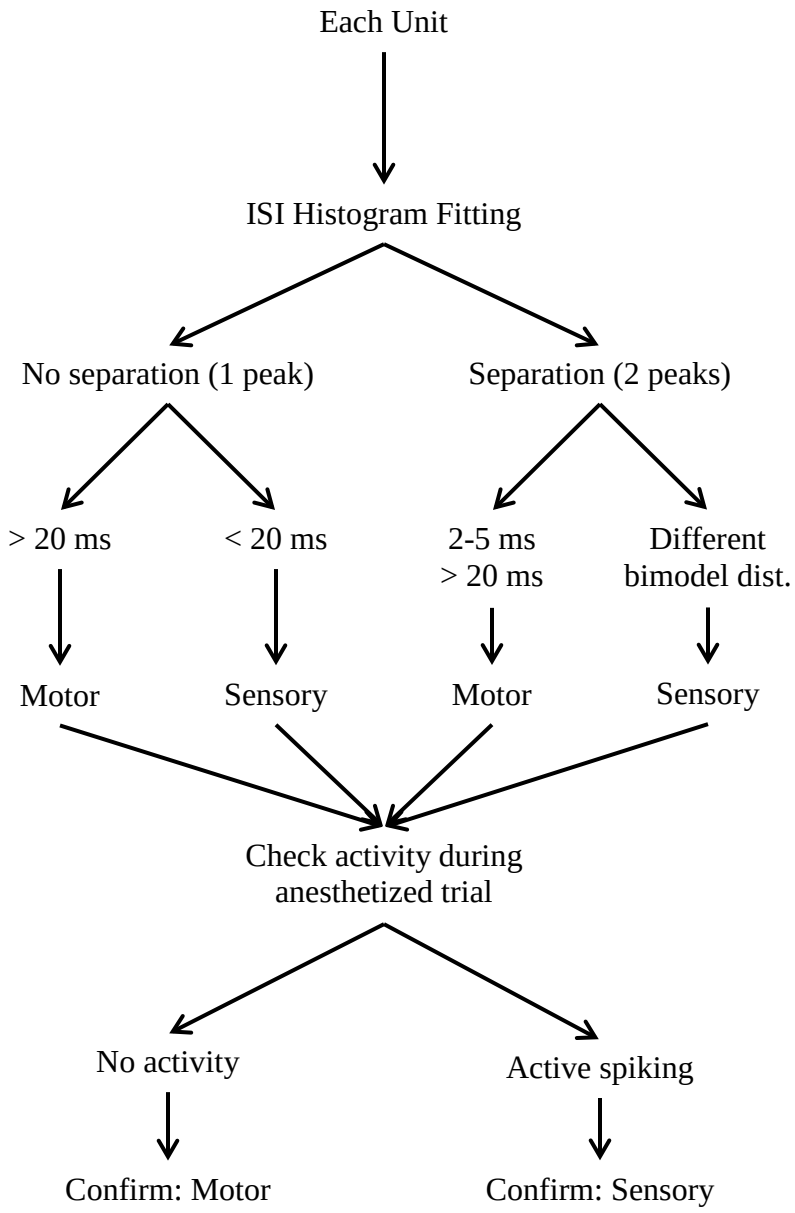

Figure 2.1. Flowchart of unit classification. Shown is a flowchart describing the algorithm for classifying units as motor or sensory and confirmation.

2.1.2 Signal-to-Noise Ratio Definition

The signal-to-noise ratio (SNR) is an important metric to define signal stability over time (Figure 2.2). The signal amplitude is defined as the average of the absolute maximum amplitude of all recorded action potentials related to one unit. Because the action potential is biphasic, the absolute maximum value may occur at a positive or negative voltage. The noise is determined by a confidence interval of 99.7% (three times the standard deviation) of non spike-related data. The SNR for a given unit is defined as the signal amplitude divided by the noise estimate.

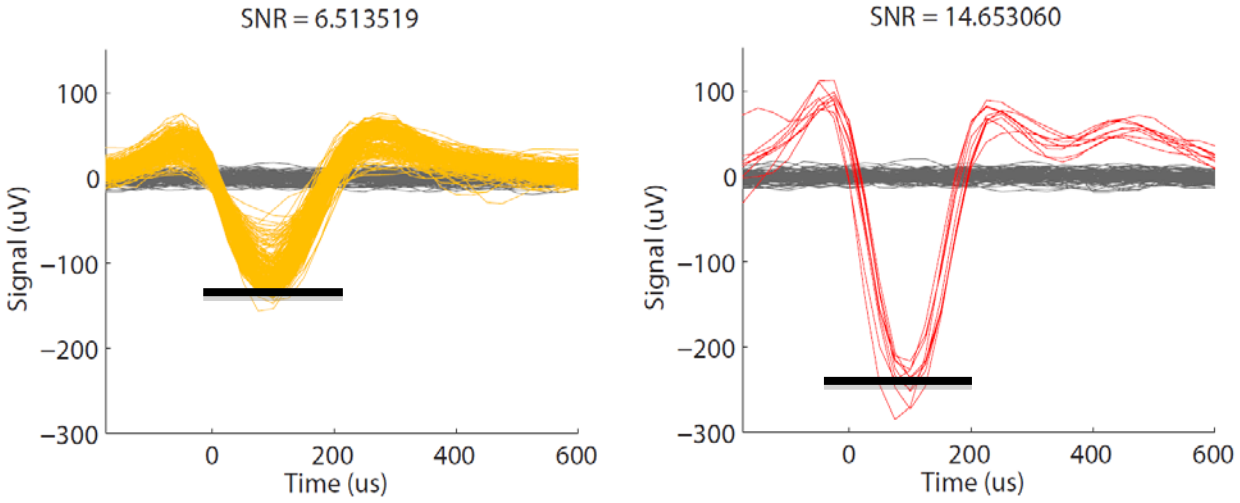

Figure 2.2. **Examples of action potential with calculated SNR.** Two examples of units with denoted SNR value, as characterized by their representative action potential. The "signal" measurement is marked (average of absolute maximum voltage of action potential) by the black line.

2.1.3 Unit Yield Definition

Unit yield is defined as the number of active channels with modulating motor-related activity. However, the number of recording sites may be smaller than the number of neurons recorded since each site may detect signals from multiple single neurons. In this study, unit yield must be defined further. Unit yield is determined only after the first two rounds of analysis described above; units only count towards yield if they are classified as motor units and have an SNR measured greater than 1.2. While the cutoff of 1.2 is relatively arbitrary, anything smaller would be considered a very poorly isolated unit and may not be useful for decoder applications towards the development of a neural prosthetic nor for physiological and anatomical studies.

Yield can also be quantified as the number of units per functioning electrode. This is to compare the number of units based on electrode specifications, such as site size and depth within the spinal root tissue.

2.2 ELECTRICAL IMPEDANCE

Electrode recording sites can be influenced by a number of biotic and abiotic responses. Biotic responses include inflammatory response, such as astrogliosis (abnormal increase in number of astrocytes due to trauma), recruitment of microglia and macrophages to the insertion site, and accumulation of scar tissue, while abiotic responses include physical changes in the electrode such as damaged insulation, corrosion, and changes at the tip surface [62, 63, 64, 65]. Electrode degradation, neural degeneration, insertion damage, and immune responses can all have effects on structural and recording properties of microelectrodes.

Some studies have shown that interface impedance can be used as a preliminary model to infer electrode-tissue interface stability, viability, and durability [65]. As present electrode arrays undergo a series of electrical, chemical, and physical change during implantation, changes in the recording site can be monitored by measuring the effective impedance; microelectrode impedances can play a role in the monitoring of low amplitude and high-resolution extracellular neural signals. Biotic and abiotic failures occur throughout the lifetime of an implant with varying degrees of intensity, and it is important to find a way to reliably quantify failure mechanisms over time and predict them accurately.

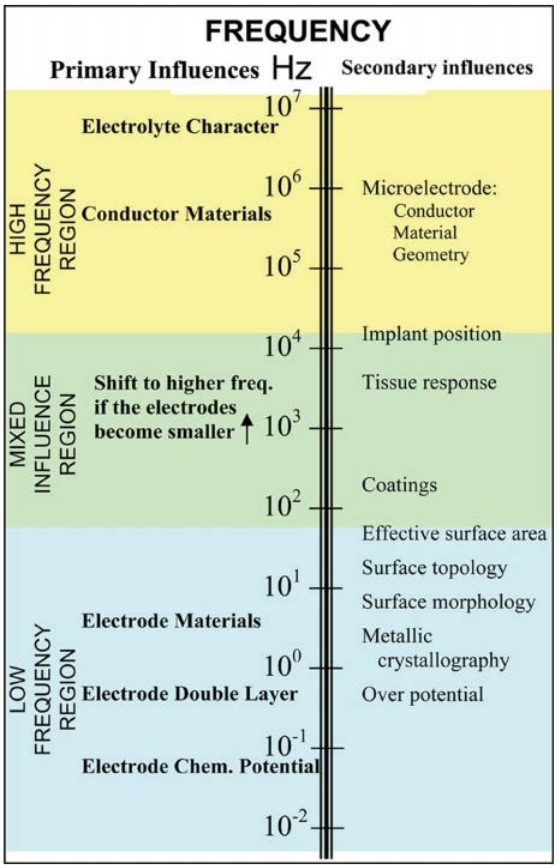

Figure 2.3. Effects on electrode impedance as a function of frequency. Shown as primary and secondary factors that can dominate behavior of bioelectrode impedance characteristics [66].

Electrical impedance, in basic terms, is a measure of the restriction of the passage of current within a circuit, analogous to electrical resistance in direct current. Impedance is denoted by both a magnitude and a phase angle, representing the phase shift of capacitive or inductive elements within the circuit that change with frequency. The magnitude and phase are measured across a range of frequencies and can be used to evaluate the electrical characteristics of an interface. Frequency range is dependent on features of interest (Figure 2.3) [66], ranging from 10 Hz to 100 kHz. To quantify electrode impedance, a small sinusoidal current (with fixed voltage) is applied at each frequency and the output is measured across the electrolytic medium.

2.2.1 Quantifying microelectrode functionality by impedance testing

Prasad et al. [65] presented a functional and electrical analysis of chronic tungsten microwire array implants in the brains of rats. The methods were developed by coupling neuronal function with the electrode's electrical properties in an attempt to gather deeper insight on electrode performance and failure modes. By measuring day-by-day changes, the study was able to observe daily biotic and abiotic changes that can occur during chronic implantation. Daily impedance measurements, only at 1 kHz, were taken to provide some understanding of interface changes on a long-term basis. The goal of the project was to investigate any functional relationships between electrical impedance and neuronal unit yield.

The microwire arrays showed steady increases in impedance following implantation, with maximum impedances at around 150-200 kΩ for functioning electrodes after about two weeks. After the one-month period, impedances did not change more than 50 kΩ per week. However, individual sites increased at different rates, which were observed by large standard deviations in

daily impedance plots. The tungsten microwire arrays had low impedances due to large recording site size, calculated to be approximately 7854 μm^2.

The study showed that units were best detected from electrodes with impedance in the range of 40 to 150 kΩ. Electrodes yielded low numbers of recorded units in the first few days after implant, accompanied by low impedances (< 40 kΩ). According to Prasad et al., low impedances reduced the ability to localize and isolate individual neurons due to increased "listening sphere" of electrodes. As impedance progressively increased, maximal yield occurred for each array, often around 2 weeks, when a sharp decrease was common throughout all animals except those that had a consistently low yield. These impedance and unit yield trends could be modeled across all animals; a Gaussian model was fit to the data to predict future electrode performance. While this prediction is far from perfect because of the many factors involved at the interface, it was possible to gain some knowledge about what to expect on a daily basis given an impedance measurement for a particular channel.

The Prasad et al. investigation did not report SNR trends nor any effect of site size or recording site surface area and their relationship with electrical impedance measurement. This thesis aims to expand on previous studies by examining SNR and unit yield as metrics for signal quality and checking any influences from impedances, as well as the results of varying recording site size for neural recordings in the ventral root.

3.0 SIGNAL QUALITY OF CHRONIC VENTRAL ROOT RECORDINGS

3.1 INTRODUCTION

The objective of the study in this chapter is to evaluate the neural recording ability of floating microelectrode arrays implanted chronically in feline ventral roots as assessed by unit yield and signal-to-noise ratios over time. The signal quality and stability are analyzed after confirming motor-related neural signals in the spinal roots recorded during natural activities. Signal quality is also compared over a number of various exposed tip lengths, or site sizes, to determine ideal electrode design.

The experimental setup of this study is based on using a feline model. Cats are one of the most common animal models used for these types of experiments because of their physiological similarity with the human sensorimotor and nervous systems. Cats are the smallest animals that can physically accommodate the electrodes required for this study. In general, there is a long history of using cats for neural recording studies, and leveraging this information is vital for designing current studies. Adult male cats (n = 9), weighing between 3 and 5 kilograms, were used for these experiments. All experiments were approved by the University of Pittsburgh Institutional Animal Care and Use Committee and the US Army Medical Department Animal Care and Use Review Office.

3.2 EXPERIMENTAL METHODS

3.2.1 Floating Microelectrode Array Design

The floating microelectrode array (MicroProbe, Inc.) is a direct descendant of the 'hatpin' electrode technology used by Hoffer and Loeb [HofferI, HofferII, HofferIII, Loeb 1987]. The FMA (Figure 3.1) uses conventional 'stiff' microelectrodes mounted in a ceramic substrate with a flexible set of lead wires, allowing the array to "float" with the neural tissue. It is the only commercially available microelectrode technology that allows customization of electrode lengths, which are between 2.3 and 3.5 millimeters, as well as exposed tip length (or site size). The depths needed to access the ventral root are deeper than the 1.0 and 1.5 millimeter electrodes available on Utah arrays, another commonly used microelectrode array.

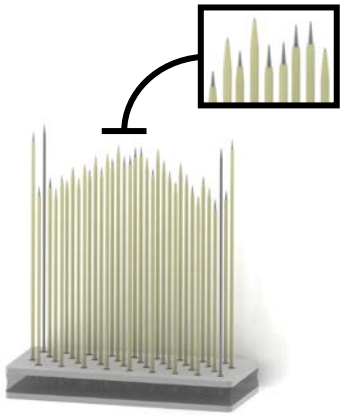

Figure 3.1. Diagram of floating microelectrode array. Shown is a diagram of an FMA with a variety of electrode lengths, along with a close up on the varying exposures at the tips.

The geometry of an electrode may have a strong impact on the quality and number of neurons recorded. For recordings from nerve axons, these dimensions are important for having a node of Ranvier within range of the electrode. The site sizes were customized to be a variety of depths between 25 and 160 μm to investigate the effect of tip length on unit recordings.

3.2.2 Surgical Implantation

The cat was put under deep anesthesia by intramuscularly applying ketamine (20 mg/kg) for initial induction; the animal continuously inhaled isoflurane during the extent of the surgical implant. Once the animal was confirmed to be at a surgical plan of anesthesia as assessed by the absence of the withdrawal reflex, the implants began. After incisions through the skin of the left leg, 8 to 10 pairs of EMG wires (from Ardiem Medical, Inc., or in-house using multi-stranded stainless steel wire from Cooner Wire Company) were placed on or in the belly of selected muscles: biceps femoris (knee flexion), gluteus medius (hip extension), lateral gastrocnemius (ankle extension), medial gastrocnemius (ankle extension), rectus femoris (knee extension), anterior sartorius (hip flexion), semimembranosus (hip extension), semitendinosus (hip extension), tibialis anterior (ankle flexion), and vastus lateralis (knee extension). These muscles are related to different phases in the step cycle and are located throughout the hindlimb of the cat. The extra wire was looped carefully and placed under the skin; the incisions were sutured closed, with all wires enclosed. Only the connector with access to all EMG wires was left loose through a skin incision at the top of the back.

A five-contact nerve cuff was also placed around the sciatic nerve. The wire for this connection was included in the EMG custom connector.

After all EMG wires and nerve cuff were implanted, a laminectomy (Figure 3.2A, B) was performed to expose the spinal roots at the lumbar segments 6 (L6) and 7 (L7). This procedure was done through a small skin incision at the top of the back above the segments of interest. The paraspinal muscles were retracted and the rest of the vertebral bone was left intact. Once the spinal roots were exposed, the FMA (32-channel [36 pins], Figure 3.3A) was prepared for insertion. A vacuum pump was used to hold the array above the spinal root so it could be positioned correctly, while pneumatic-actuated inserter (Blackrock Microsystems), a rapid insertion mechanism, was set for optimized depth and insertion speed. Using the pneumatic inserter, the FMAs were implanted into the tissue, and intraoperative recording was done to confirm the location in the ventral root. The FMA must travel through the dorsal root (Figure 3.3B) to get to the ventral root. Under deep anesthesia, only sensory units (in dorsal roots) remain active, while there should be no spontaneous motor-related activity in ventral roots. The FMAs were advanced further with the pneumatic inserter until only shallow channels had very little or no sensory activity remaining. This insertion was done for ventral roots of both L6 and L7 spinal roots (Figure 3.2C). All wire bundles were attached to the dura with 8-0 suture.

After implantation of all the recording equipment (10 EMGs, 2 FMAs, and 1 nerve cuff), an extra ground wire was wrapped around a bone screw in the iliac crest and an extra reference was placed in epidural space near the spinal cord. With everything implanted, all connectors and external wires were gathered into a custom housing unit (Figure 3.4). This “backpack” was mounted subcutaneously with a foundation implanted over the iliac crest. With a custom mating board that allows flexible reference and ground selection, this robust connector scheme can accommodate up to 14 bipolar EMG channels, 3 FMAs (96 channels), and extra ground and

reference electrodes. The studies here, as stated earlier, use 8 to 10 bipolar EMG channels and 2 FMAs (64 channels) along with extra implanted ground and reference wires (Figure 3.5).

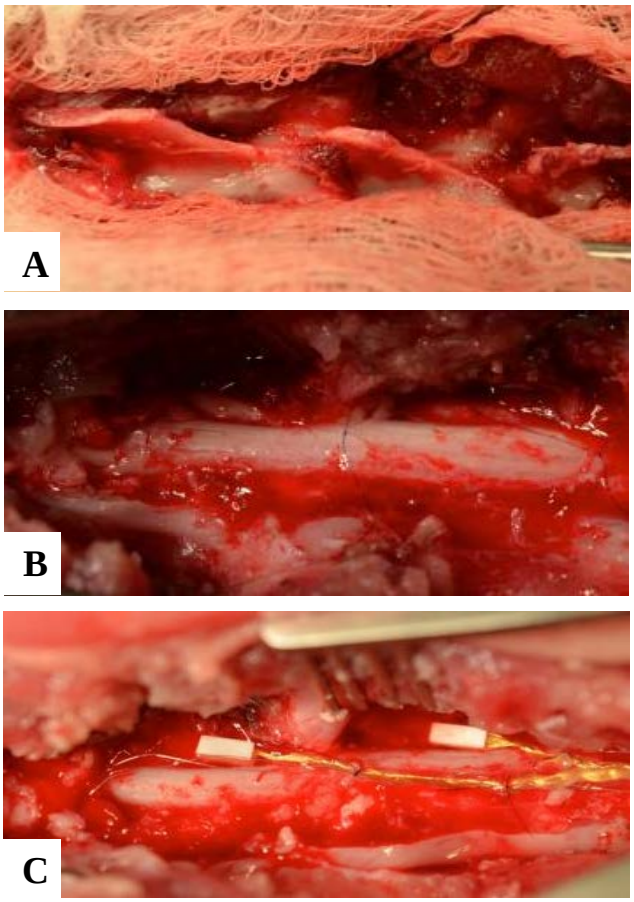

Figure 3.2. Images from implantation surgery. A. Lumbar vertebrae before laminectomy, B. Lumbar section of spinal cord and lumbar spinal roots exposed after laminectomy, C. Floating microelectrode arrays implanted in left spinal roots at L6 and L7.

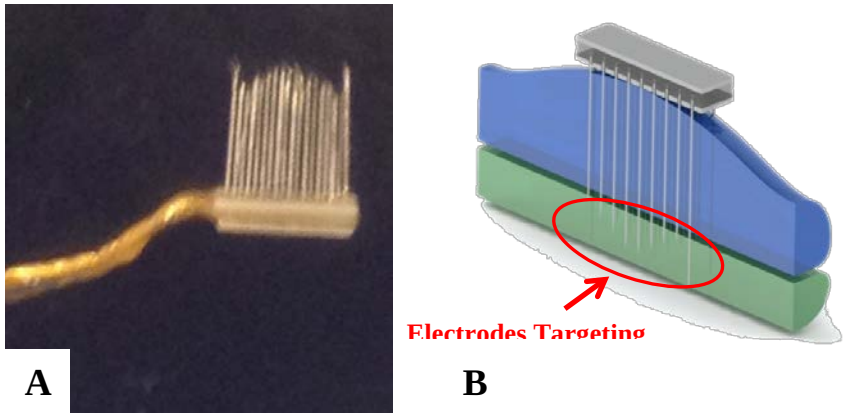

Figure 3.3. Floating microelectrode array and insertion. A. Example of floating microelectrode array before insertion, B. Diagram displaying electrodes traveling through the dorsal roots to target ventral roots and reach segregated motor-related activity.

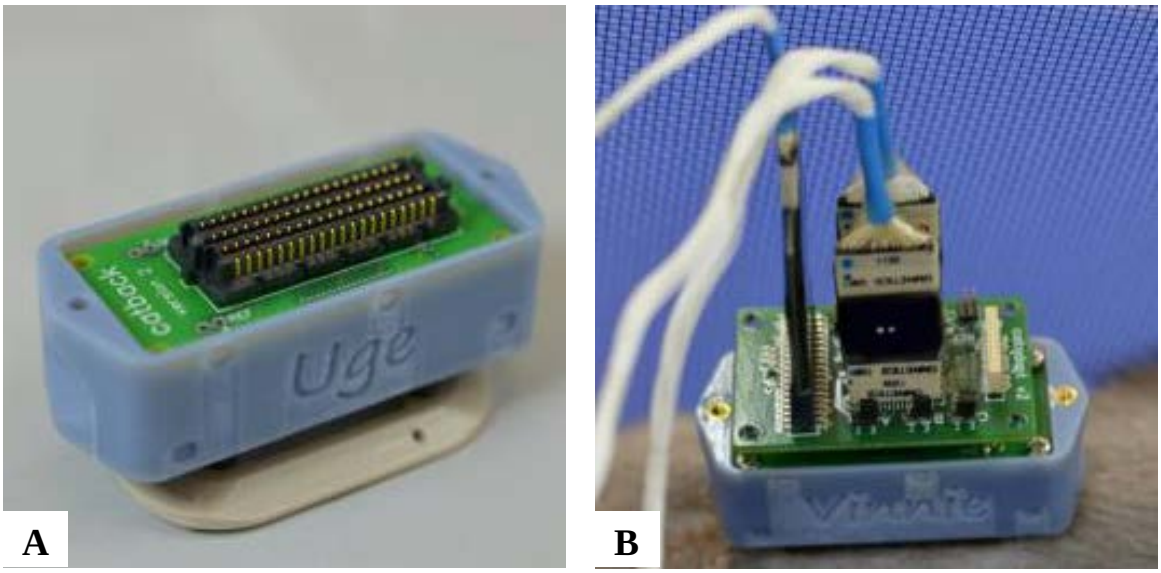

Figure 3.4. Cat backpack. A. Example of cat backpack, a 3D-printed housing unit containing all external wires and connectors from implanted recording equipment, B. Cat backpack with all connections necessary for recording from 10 EMGs, 2 FMAs, and a 5-contact nerve cuff.

Thirty minutes prior to the discontinuation of anesthesia, animals were given buprenorphine (0.01 mg/kg) intramuscularly. After surgery, the cat was allowed to wake up and recover until they were able to walk freely and without a noticeable limp, which was only about three to four days. Buprenorphine was provided every 12 hours for three to five days, post operation. This quick recovery time allows recording within a week of the implant.

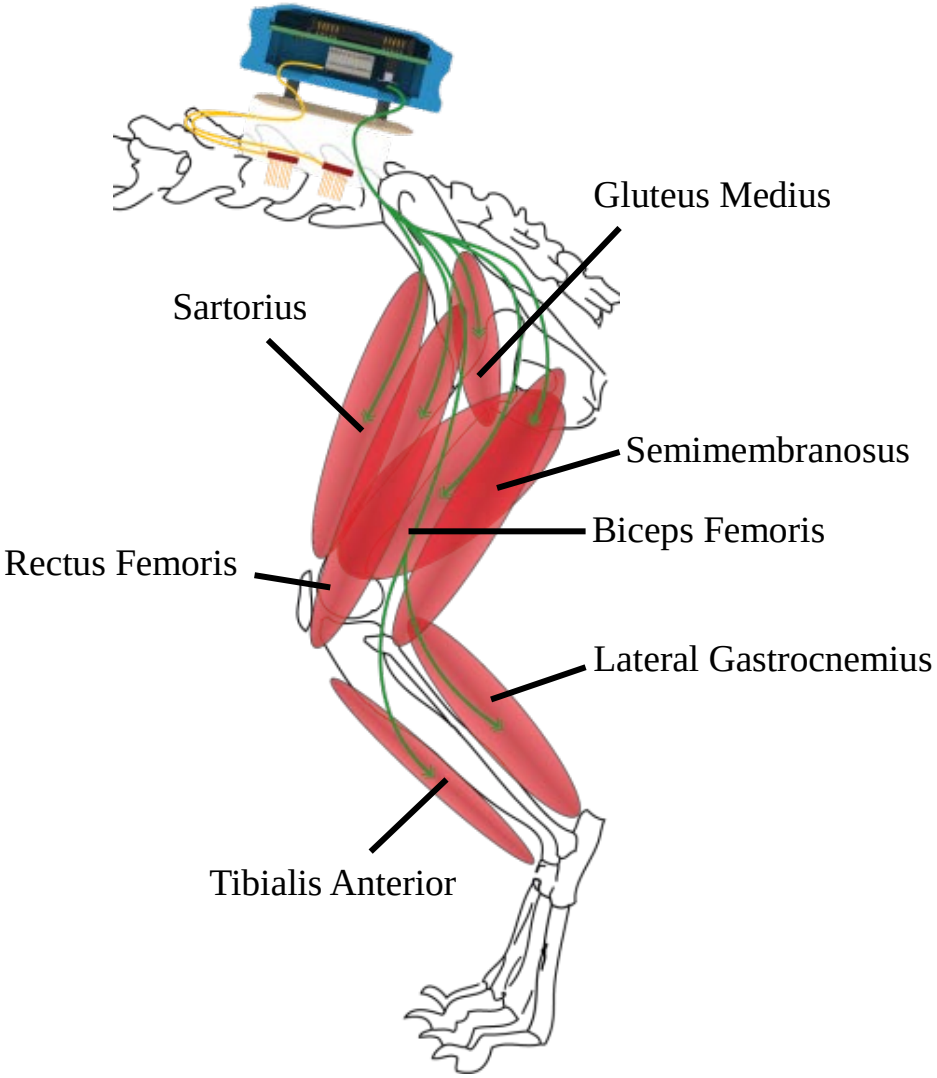

Figure 3.5. Diagram of cat leg with implants. Shown are 2 FMA implants at L6 and L7 spinal roots (yellow with red), EMG wires to 7 leg muscles (green), and external connections within the custom cat backpack (top, in blue). Muscles not shown: Medial Gastrocnemius, Semitendinosus.

3.2.3 Spinal Root Recordings

Before a cat was considered for implantation, it was trained to walk on a dual-belt treadmill at speeds ranging from 0.2 meters per second up to 1.4 meters per second. Cats are trained every day to walk constantly without trying to jump out the enclosed area or run into the back wall because they may refuse to walk. Food is often used as motivation during early stages of training, but later on, the cats are fed once their day of exercise is completed. After array implantation, food is withheld during treadmill trials, as anesthetized trials are often completed immediately after.

Once the cat had recovered from implantation surgery, neural recordings were compiled during awake and anesthetized trials. Neural signals from the microelectrode arrays were recorded with a signal processing system (OmniPlex, Plexon, Inc.) at 40 kHz and monitored constantly during all trials. EMG signals were also recorded; the sampling frequency for EMG channels was inconsistent between subjects and varied from 5 to 20 kHz. Kinematics were gathered by using markers, video tracking software (Cineplex, Plexon, Inc.), and a number of installed cameras in the testing room. After connecting headstages to the custom backpack and mating boards, the cat was ready for neural recordings.

Awake trials ideally consisted of three testing blocks. First, the cat would walk on the treadmill (Figure 3.6) for up to five minutes at speeds ranging from 0.2 to 1.4 meters per second (usually slower right after surgery, but up to maximum speeds within a week). The second block was a standing trial, when the cat would stay still, either sitting on the treadmill or standing on all four legs. Lastly, signals were recorded as the cat stood on his hind legs while leaning upon a wall of the enclosure around the treadmill. The cats did not always stay in this bipedal stance for

very long, so this block was often short, but this block provided a stance with a constant force upon certain muscles. Awake trials were performed three times per week.

Figure 3.6. Cat on treadmill. Single unit recordings performed during treadmill locomotion for up to five minutes at a range of velocities from 0.2 to 1.4 meters per second.

Of the three times that awake trials were done each week, anesthetized trials followed at least two. After completing the treadmill blocks, the cat was lightly anesthetized with an injection of dexdomitor (40 µg/kg). After the anesthesia had taken effect (typically 5-10 minutes), additional trials were performed. First, neural signals were recorded in a "quiet" session, with no stimulus, for up to approximately one minute. Second, the implanted leg (left) was moved in a "ramp and hold" pattern; a member of the lab would flex the entire leg at a moderate pace, hold it flexed, then fully extend the leg at the same pace, and holding it in the position. The leg would continually be maneuvered in this pattern for up to a minute while neural

signals were recorded. Third, recordings were done while the leg was moved in a random pattern; a member of the lab would manipulate the leg in random motions, flexing and extending different joints at different speeds, as well as cycling the leg forwards and backwards. Lastly, another quiet trial was recorded. These movement recordings under anesthesia provide a way to compare motor and sensory recordings during leg locomotion between awake and anesthetized trials.

While the cat remained anesthetized, electrical impedances of the FMAs were collected. Impedance recordings and analysis are described in Chapter 4.

3.2.4 Spike Sorting

During recordings, an amplitude threshold was set on each electrode channel above the noise floor, and a spike event was stored when this threshold was crossed. Each spike event consists of a time stamp and a snippet of a voltage data before and after the threshold crossing, making up the spike's waveform. All spike events are stored, regardless of the number of different units on an individual channel.

After all recordings, data was preprocessed for spike sorting. All blocks for a single day were sorted together, as units typically remain on the same channel for all blocks on that date. This also enabled analysis of differences between awake and anesthetized trials, as motor units should only show activity during awake trials, while sensory units fire during awake and anesthetized trials. All files on one day were merged (PlexUtil, Plexon, Inc.) and loaded into spike sorting software (Offline Sorter, Plexon, Inc.). Cross channel artifacts were invalidated, as artifacts present on at least 25% channels with spikes and within 75 μs were removed. The

results of calculating the first three principal components of the snippet waveforms were visualized. Clustering and spike sorting was performed by hand until all waveforms were determined to belong to the activity of a unit or as external noise (Figure 3.7). Many channels contained activity from multiple single units, and these clusters were manually verified by hand sorting.

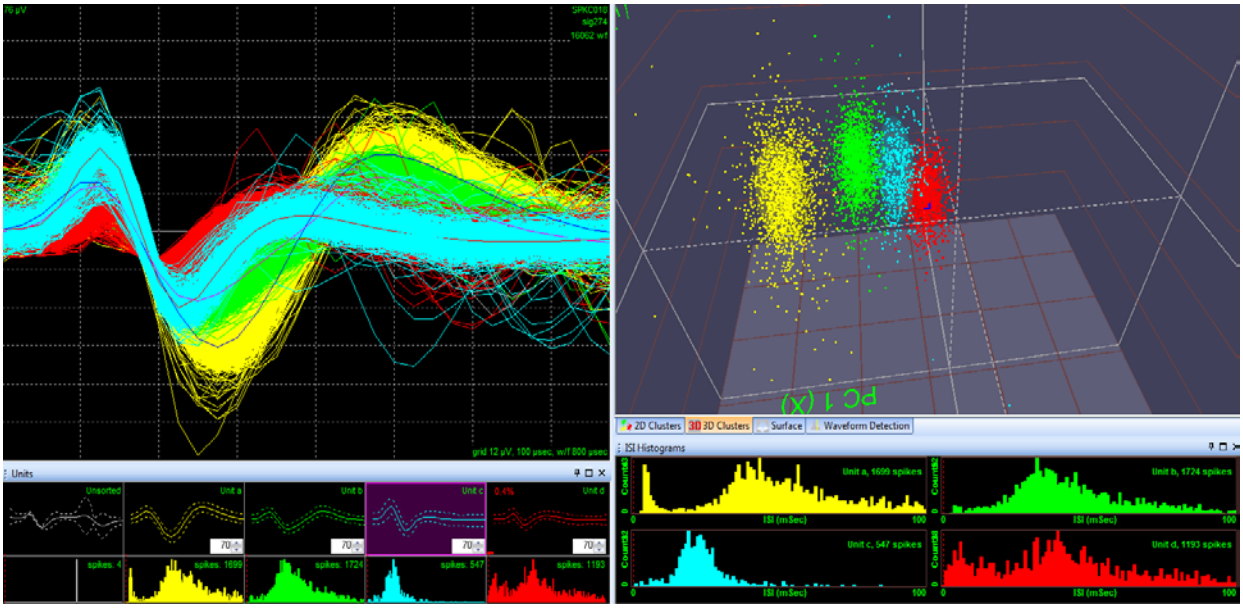

Figure 3.7. Example of hand-sorted channel. In Offline Sorter (Plexon, Inc.), snippet waveforms were sorted manually on each channel from visualization of principal component analysis in three dimensions. This particular channel contains 4 single neurons; noise waveforms are invalidated and not shown.

3.2.5 Classification of Units

With each channel and each block sorted, the unit waveforms were classified by type. Motor and sensory-related neural signals were separated by the algorithm described in section 2.1.1. Each sorted unit found during an awake trial was examined individually using three steps: ISIs were fit

to a statistical mixture model, activity was compared during a corresponding anesthetized trial, and classification was matched with other units on the same channel. If a unit had ISIs that matched a Gamma distribution with a peak at greater than 20 milliseconds (with a possible second peak at 2 to 5 milliseconds, representing doublets), only showed modulating activity during awake trials while remaining absent during anesthetized trials, and belonged to a channel also containing other motor-related units, then the unit was considered to be motor. Otherwise, the unit was classified as sensory and not analyzed further.

After classification, the signal-to-noise ratio (SNR) was calculated, as described in section 2.1.2. Units with an SNR greater than 1.2 were counted towards the unit yield, as described in section 2.1.3. SNR and unit yield values were tracked longitudinally and used as metrics to quantify long-term neural recordings in the ventral root.

3.2.6 Exposure Site Area Calculations

The exposure site area was calculated based on specifications from MicroProbes for Life Sciences, Inc. The electrode tip is modeled as a conical frustum, or right cone with the top cut off. The radius at the top of the frustum is approximately 4 µm (+/- 20%), while the diameter at the base of the electrode shaft is 75 µm. The etched taper from shaft radius to tip radius is 2 mm long. The height of the frustum exposed is given as the site size and ranges from 25 to 160 µm (+/- 20%).

Using these values, it is possible to calculate the approximate surface area of the exposed part of the tip. The area calculations are shown in Table 3.1. Group 1 cats (W, V, U, and T) had

site sizes of 25, 50, 100, and 150 µm while group 2 cats (S, R, Q, P, and O) had site sizes of 40, 80, 120, and 160 µm, as shown in the table.

Table 3.1. Site sizes and corresponding recording surface area. Trigonometry was used to calculate recording surface area from the site size and electrode shank/taper specifications supplied by MicroProbe, Inc.

Site Size (µm)	Recording Surface Area (μm^2)	Group
25	711.6	1
40	1139.9	2
50	1438.7	1
80	2398.0	2
100	3090.2	1
120	3824.5	2
150	5004.9	1
160	5419.4	2

3.3 RESULTS

This study was undertaken to establish the ventral root as a viable target for long-term neural recording and a future option for the control of motor neuroprosthetics. By implanting FMAs into the lumbar spinal roots to target the ventral root, motor-related activity was recorded during awake and anesthetized trials. After manually spike sorting neural activity, SNRs and unit yields were calculated.

3.3.1 Confirmation of Motor Recordings

The number of channels with recorded units classified as motor or sensory for each array is shown in Figure 3.8. Each subject had two arrays, which are labeled as 6 or 7 based on the location of the array in L6 or L7, respectively. The data shown in this figure represents an exemplar trial for each cat; for example, on an exemplar recording day, cat W had 16 channels out of 32 with modulating motor-related activity on the array implanted in the L6 spinal roots with 1 (presumably shallow) channel with sensory activity. The number of channels does not accurately portray the unit yield, as multiple single units were often found on a single channel. Arrays are sorted here by the number of motor-related channels.

Motor-related activity was found on a majority of the implanted arrays, with only a few (R-7, Q-7, O-7) with only sensory or no activity. Most of the array implants performed successfully; many of the active channels contained activity from multiple single units. In the case of R-7 and Q-7, the FMA was not inserted deep enough and all recorded activity was from the DRG. Meanwhile, S-7 and O-7 represent poor implants; the array may have missed the spinal roots entirely or broken during the insertion procedure.

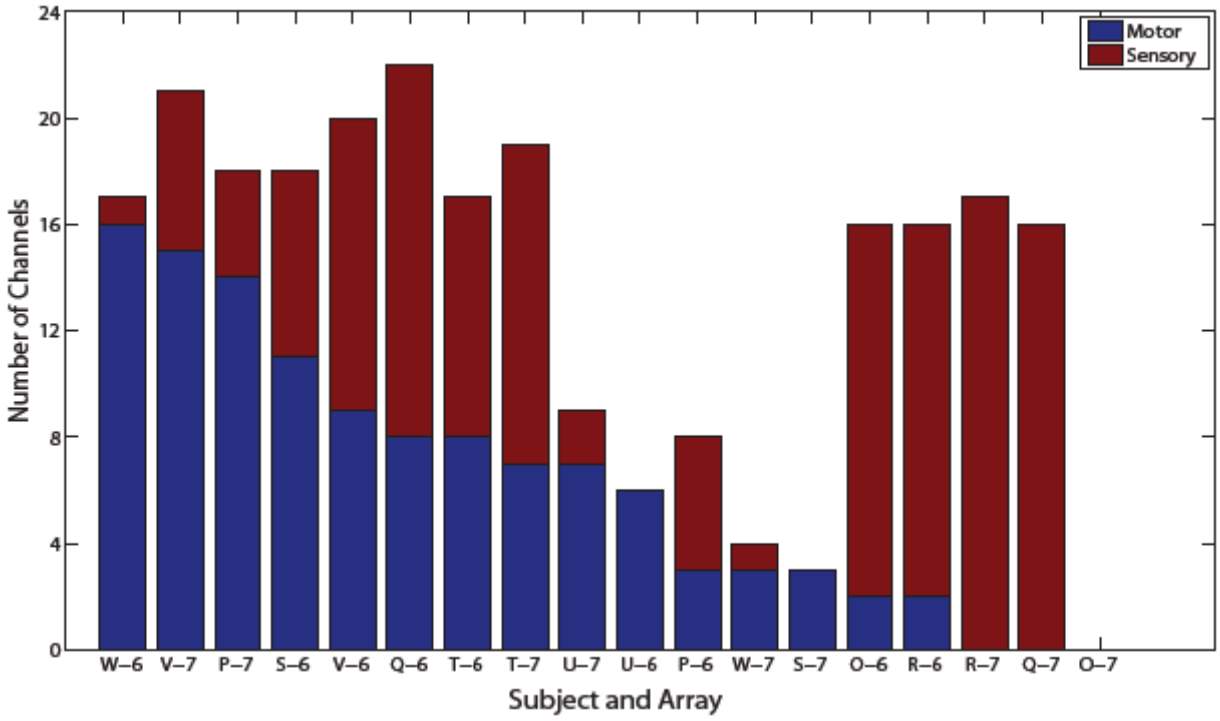

Figure 3.8. Channels classified as motor or sensory-related activity. Shown is the number of channels classified as motor or sensory on each array. The animal is denoted by the letter, while arrays in L6 or L7 are labeled as 6 or 7, respectively. Results are sorted by number of motor-related channels in descending order.

3.3.2 Signal-to-Noise Ratios

The SNRs were calculated for all hand sorted units classified as motor, on all channels and on all blocks. These were compiled by week to show the stability of SNR over time in Figure 3.9. The median SNR (shown by the red line) remained at 2 or higher over the lifetime of all implants. In the first four weeks, very high SNR values were observed in a number of cats, shown by the outliers denoted by red "+" signs. With a majority of SNRs greater than 2, it was shown that the implanted FMAs in spinal roots could measure action potentials from single neurons with a useful SNR for extended periods of time.

The numbers of units and lifetimes of cats (and their arrays) are described in more detail in the next section, 3.3.3. No trials were done on week 9 of any implant.

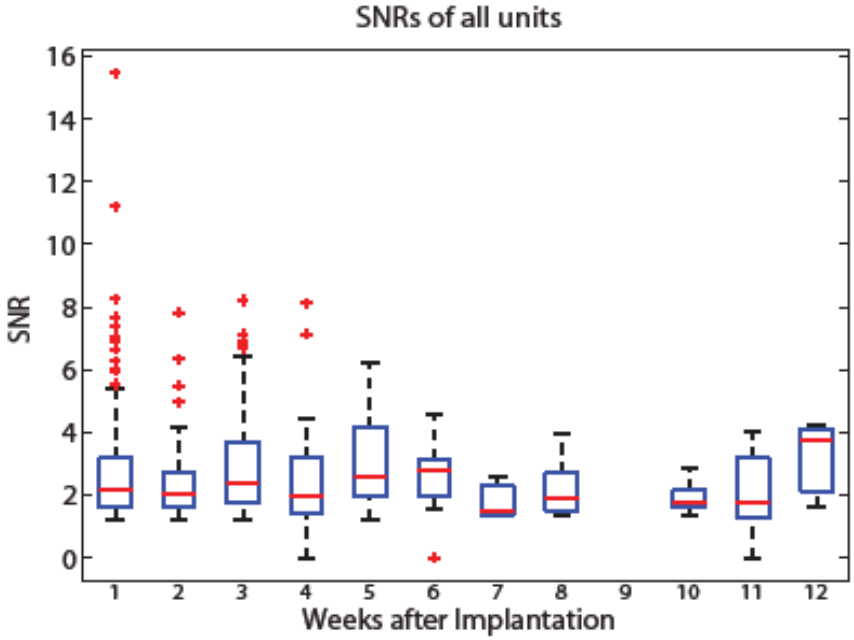

Figure 3.9. SNRs of all units classified as motor over time. Compiled by week to show stability of SNR over time. Median SNR remained greater than 2 through 12 weeks post-implant. No data was recorded on week 9 of any implant.

3.3.3 Unit Yields

After calculating SNRs for all units classified as motor, unit yield was measured by including units with an SNR greater than 1.2; an SNR lower than 1.2 would correspond to a very poorly isolated unit which is likely noise. The total number of units counted for each week was divided by the number of arrays measured from in that same week to calculate the average number of units per implanted array, as shown in Figure 3.10. The lifetimes of subjects varied, and only

available arrays were included in the unit yield calculations. The lifetimes are shown in Figure 3.11.

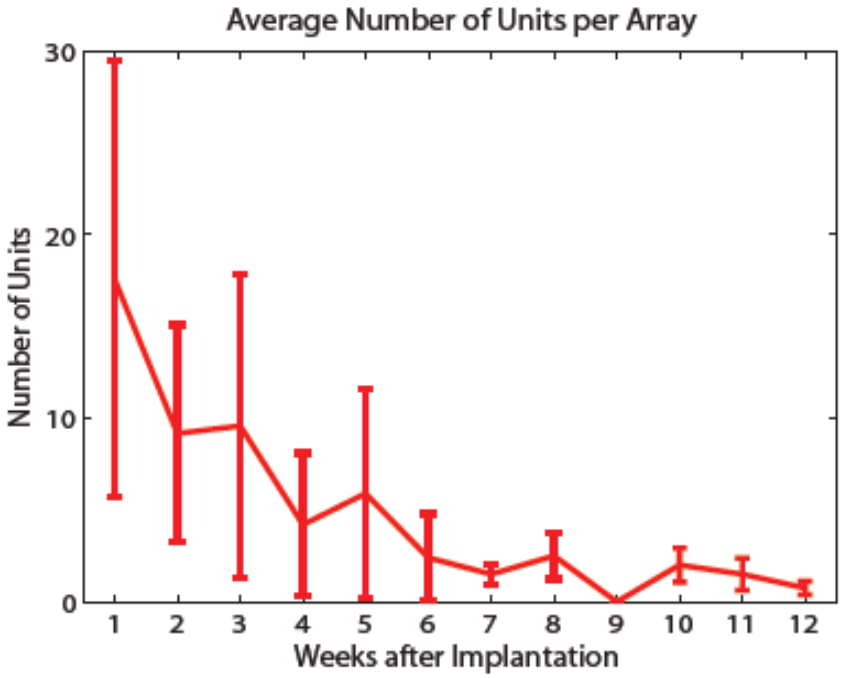

Figure 3.10. Average number of motor units per array over time. Unit yield was calculated by counting the number of motor units with an SNR greater than 1.2. These yields were normalized by the number of arrays recorded. Units were recorded through 12 weeks post-implant.

While there was nearly an average of 20 units per array in week 1, this value dropped to between 5 and 10 until week 6, where it fell further. No trials were done on week 9, hence the lack of data there, but there were still a few units remaining after week 12.

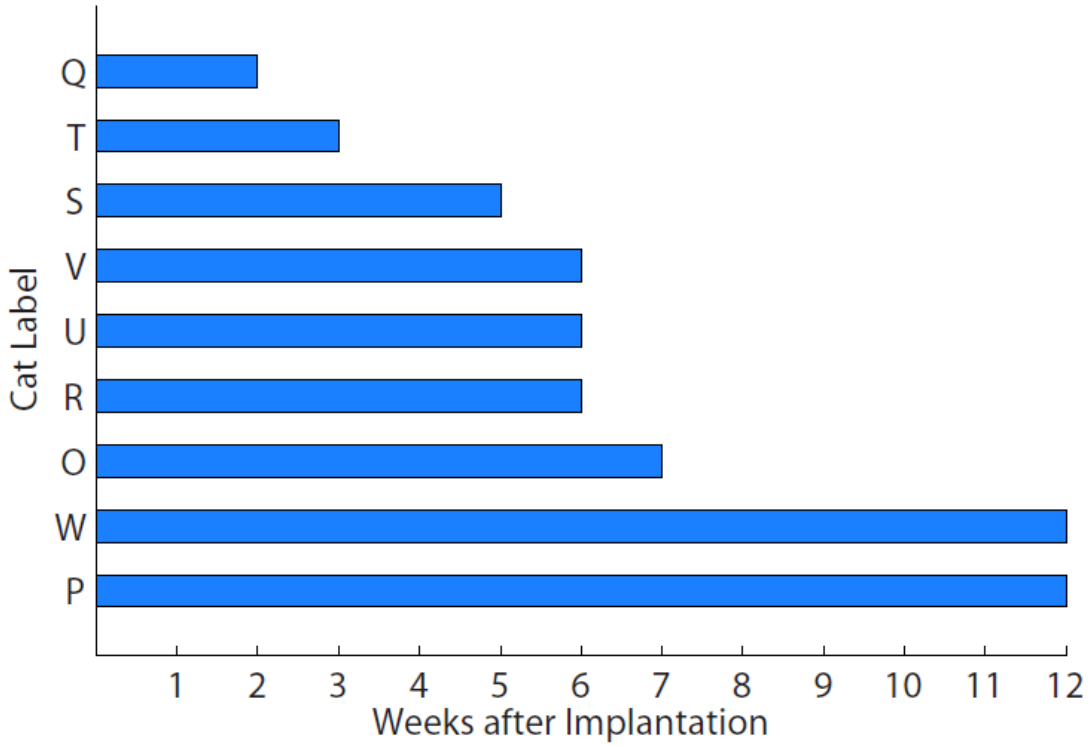

Figure 3.11. Implant periods for all cats. Cats were perfused early for a number of reasons; only W and P reached the end of the planned implant period.

Experiments were terminated prior to the planned 3-month (~12 weeks) implantation period for a number of reasons; only two cats reached the end. Cat Q's implant procedure led to a strong immune reaction and suffered from infection, while cat T had a backpack injury that lead to broken leads and arrays. Cats S, V, U, R, and O had good implants and yields initially, but there was slow signal degradation and poor yield within approximately 5 to 6 weeks.

3.3.4 Summary by Cat

The three sets of analysis were applied to an exemplar block for each cat, shown in Figure 3.12. For each cat, the units are separated into a histogram by SNR, showing the number of classified motor and sensory units and an approximation of their SNR from a singular recording session. This is an expansion upon the array analysis in Figure 3.7; both arrays from each cat are grouped together and the number of units, not just active channels, is more explicitly shown in this figure. Table 3.2 summarizes the number of motor and sensory units for each of the cats shown in Figure 3.12. Most of the cats had more motor than sensory units, as only R, Q, and O had more sensory signals on an exemplar recording day, and a majority of SNR values were greater than 2.

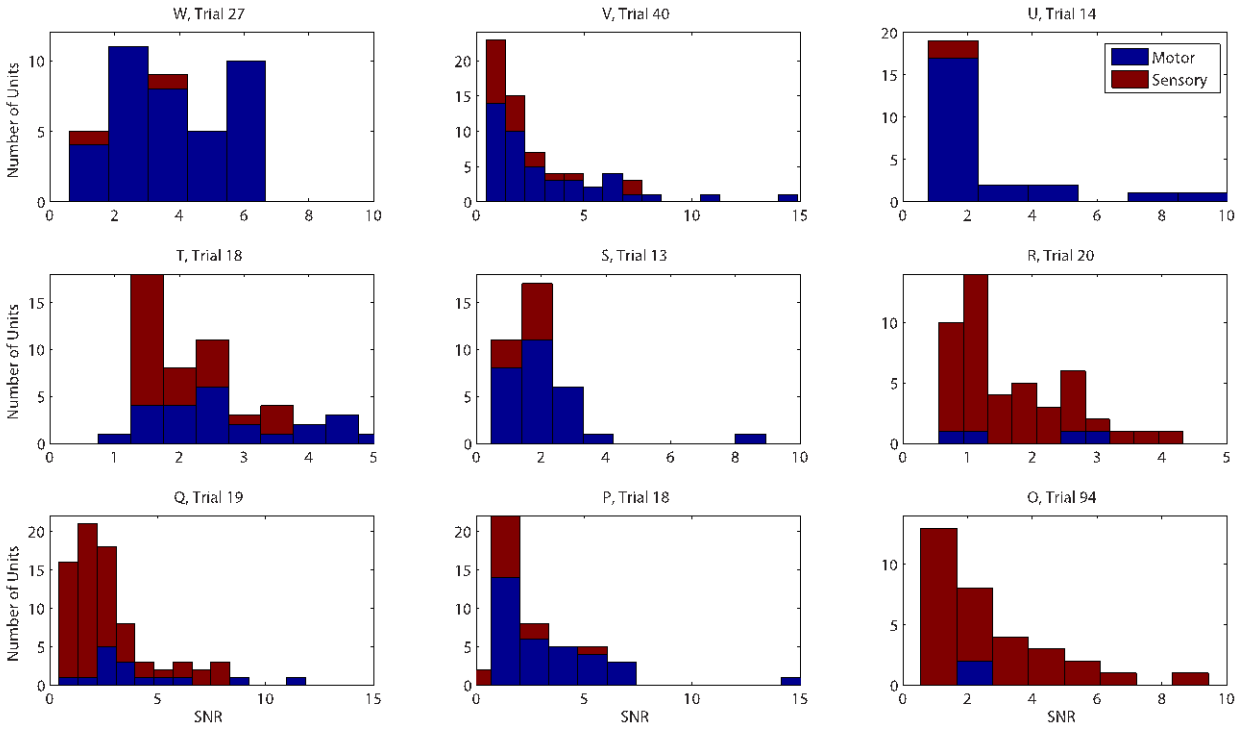

Figure 3.12. Histogram of motor and sensory units. Motor and sensory units recorded on an exemplar day for each cat are sorted by SNR and stacked to show number of units within each SNR range.

Table 3.2. Exemplar recording sessions: number of units by type. Shown are the numbers of motor and sensory units on exemplar recording sessions per cat.

Cat Label	Motor Units (VR)	Sensory Units (DRG)
W	39	2
V	45	20
U	23	2
T	26	28
S	27	9
R	4	43
Q	15	64
P	33	13
O	2	30

It can be noted that many of the earlier implants had more motor signals, while the later subjects were not as successful. Observation of perfused tissue showed implants driven through the tissue and electrode shafts bending upon further contact (Figure 3.13). In an attempt to remediate this issue, electrodes were implanted slightly shallower (based on intraoperative recordings). This led to electrodes being implanted too shallow and they recorded more DRG activity than desired.

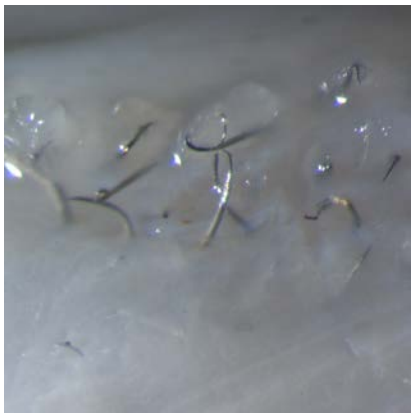

Figure 3.13. Ventral side of perfused spinal roots. Shown is an example of a perfused spinal root tissue on early implant, where the electrode tips are clearly visible, as they traveled through the ventral root and bent with further contact.

3.3.5 Site size analysis

The effects of site size on SNR and unit yield are shown in Figures 3.14 and 3.15, respectively.

There was no effect of site size upon SNR, as all site sizes recorded units with similar SNR values between 2 and 5. All site sizes also were able to record more isolated units with higher SNR, as shown by the outliers in the boxplot of Figure 3.14. There is however, a difference in total unit yield over all site sizes. The smallest site size for each group (see Table 3.1) recorded the least number of units compared to the other 3 site sizes, which recorded similar numbers of units. All site sizes were not plotted together due to the difference in total units recorded over each group.

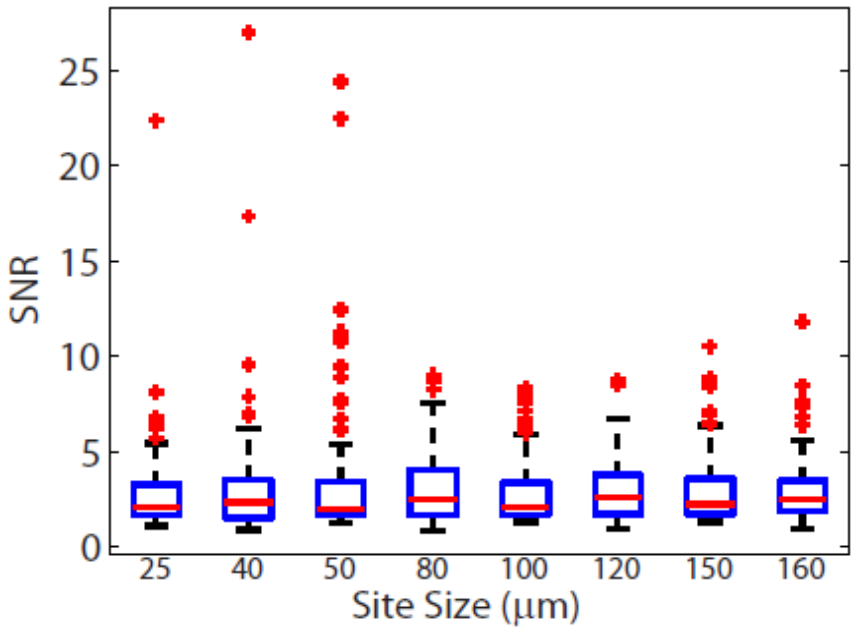

Figure 3.14. Boxplot of SNR values for all site sizes. The median SNR for each site size is denoted by the red line within each box, which is formed using the upper and lower quartile for each set of data. The red "+" symbols denote outliers and represent very well-isolated units with a high SNR.

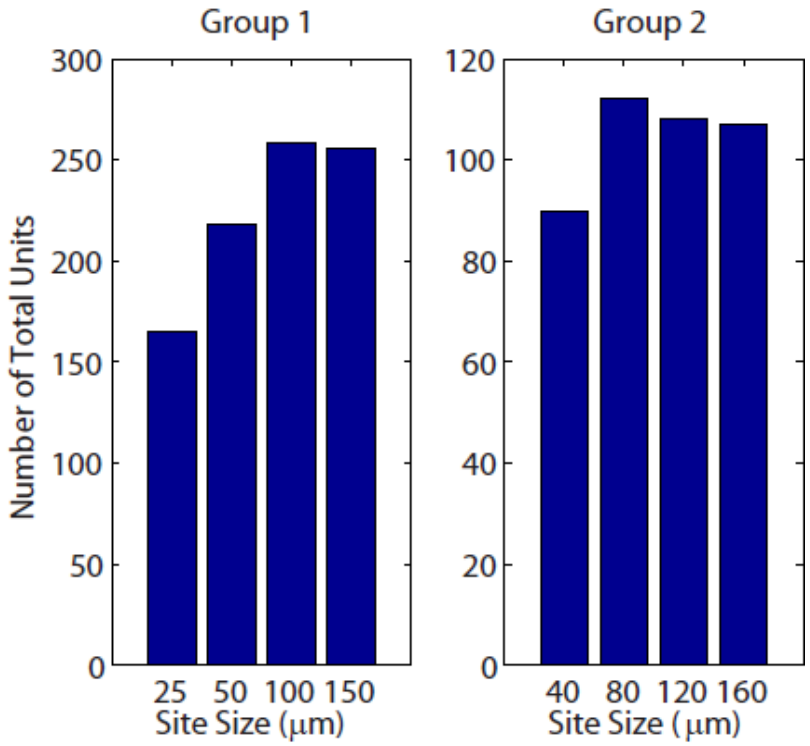

Figure 3.15. Number of total units for all site sizes. The site sizes are separated by implant group (see Table 3.1) due to the differences in total yield between the groups.

Given a site size, electrical impedance (described more in Chapter 4) can be used to diagnose functionality. Electrodes with an impedance less than 2000 kΩ were collected and separated by size to determine the average number of units recorded given a functioning electrode, shown in Figure 3.16. Electrodes with a site size of 25 μm recorded a significantly lower average of units, while the distributions for the rest of the site sizes were not significantly different.

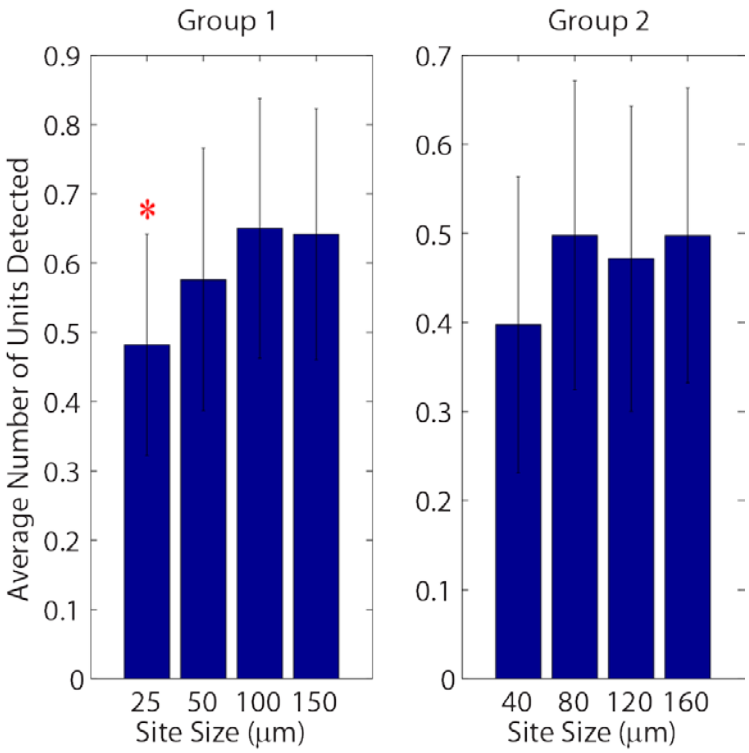

Figure 3.16. Average number of units with functioning electrode. The site sizes are separated by implant group (see Table 3.1) due to the differences in total yield between the groups. Asterisk denotes significance, with $p < 0.05$ from a one-way ANOVA.

3.4 DISCUSSION

The objective of the study in this chapter was accomplished by recording single-unit activity from microelectrode arrays in the ventral roots and assessing long-term performance, quantified by signal-to-noise-ratios and unit yields over time. On exemplar days, large numbers of well-isolated units were recorded, with up to half of channels on an array containing modulating motor activity. Some implants have successfully resulted in primary motor recordings, while others have had sensory recordings (as seen in Figure 3.12).

Over time, SNR measurements have remained consistently high even though the number of responsive channels decreased; well isolated units have been recorded steadily for up to 12 weeks, with high SNR units seen in the first 4 to 5 weeks. The unit yield remained at greater than 10 units per array for up to 5 weeks. Around week 6, the number of units per array dipped considerably. High SNR recordings from large number of single-unit motor neurons fibers in behaving cats have been achieved for up to 3 months.

Some limitations still remain; implanting FMAs through intact epineurium has proven to be difficult and required high speed methods, but has been consistently accomplished. However, electrode targeting has remained challenging to achieve on a regular basis, as seen by the presence of sensory recordings.

Implant viability has also been hard to maintain, as only 2 subjects reached the end of their implant period while sustaining units with a reasonable SNR. It is difficult to manage a large number of connectors and percutaneous wire bundles. The implant and backpack can lead to skin erosion around the connector base, as well as fluid seeping into the connector board. The fragility of the array assemblies and corresponding cables can also lead to catastrophic failure within a few weeks of implantation, particularly due to the motion of the cats. This custom backpack was a new system, and many of these issues were solved. It is performing well now and this study could not have been done with the use of the cat backpack and connector scheme.

3.5 FUTURE WORK AND CONCLUSIONS

Future plans for this work include the development of a new implant procedure from the ventral side of the spinal roots. A new strategy may allow for better targeting of the ventral roots, as it

completely bypasses the dorsal root ganglia. Better implants may lead to longer lasting implants and higher overall signal quality. The goal is to extend implants to 6 months and up to a year in the next generation of ventral root studies.

An expansion upon the results will include analysis and correlation of the recordings from the implanted nerve cuff and EMG wires to evaluate their viability as a source for neuroprosthetic control. Target muscles for each of the recorded units can be found by spike triggered averaging of EMG recordings and correlations with rectified and filtered EMG. The z-score and correlation coefficients can be used to accurately identify strong and weak target muscles across all recording sessions. These results can be used to examine decoder strategies that incorporate muscle target information.

This study has shown successful single-unit recordings from FMAs implanted chronically in ventral roots. Identifying, tracking, and decoding motor signals from the ventral root can lead to the possibility of neural control of prosthetic arms from a reliable peripheral interface.

4.0 ELECTRODE IMPEDANCE AND SIGNAL QUALITY

4.1 INTRODUCTION

The objective of the study in this chapter is to analyze signal quality of chronic neural recordings from the feline ventral roots as a function of the electrical impedance of implanted electrodes. Impedances of individual channels are measured and both SNR and unit yield are applied to develop metrics to check for influences of electrical impedance on signal quality.

The studies also look to evaluate electrode design by correlating signal quality and working impedance ranges for a variety of exposed tip sizes; the exposed tip sizes vary the recording site area. An ideal tip size would record a high number of units with high SNR reliably over time. The relationship between electrical impedance and site size is also interpreted by chronic impedance measurements for all cats, and signal quality can be analyzed as a function of site size.

4.2 EXPERIMENTAL METHODS

4.2.1 Pre-Operative Testing

Before implantation of the electrode arrays (described in Chapter 3), each array was examined and tested. After melting carbo wax (polyethylene glycol), which is used for protection of the microelectrodes during shipment, the arrays were inspected thoroughly through a microscope to check for bent or broken electrodes and the integrity of the wire bundle was also checked. While visual inspection was useful, the connections were confirmed to be intact by measuring impedances of all electrodes pre-implant. A NeuroNexus Instrumentation POD (niPOD, NeuroNexus Technologies, Inc.) was used to measure electrical impedances *in vitro* at 1k and 5k Hz with the electrode array set in a saline solution. A reference electrode was also placed in the solution and the circuit was grounded.

After pre-operation impedances were measured, the array was visually inspected a final time and rinsed with deionized water before being packaged for sterilization. Sterilization was completed by ethylene oxide (EtO) methods. EtO gas infiltrates packages and products to kill viruses, bacteria, fungi, and any other microorganisms that may linger from production or packaging processes [67]. It is not recommended that microelectrode arrays be sterilized by autoclave; the high-pressure saturated steam applied during autoclaving requires special housing and support for the array due to the fragile nature of the design [68]. The sterile arrays were implanted into the spinal roots of cats, as described by the surgical procedure in section 3.2.2.

4.2.2 Impedance Measurements

Section 3.2.3 described the methods for spinal root recordings during treadmill locomotion and under anesthesia. Immediately after these recordings, while the cat remained under anesthesia, impedances were recorded from the implanted floating microelectrode arrays. The niPOD was used to check the impedances at frequencies of 1k and 5k Hz for each of the 32 channels on each of the 2 arrays. The array's reference and ground electrodes were employed as reference and ground points for the impedance measurements.

The niPOD was used for impedance measurements for the first 7 subjects (W, V, U, T, S, R, and Q). However, there were limitations to the speed of measurements and the number of measuring frequencies. The Multi Autolab (Eco Chemie, Metroohm group) was used for impedance analysis for 1 subject (P); the CompactStat (Ivium Technologies) was used for some trials for subject P and for subject O. For both the Autolab and CompactStat, measurements were taken at 17 different frequencies ranging from 10 to 100k Hz. Impedance measurements took up to 40 minutes, and the cat was given small dose shots of dexdomitor to maintain its anesthetized state throughout recording sessions.

The subject was injected with antisedan (0.3 mg/kg) to reverse the sedative effects of dexdomitor after all impedance measurements were taken, in addition to the neural recordings from Chapter 3. After waking, the cat was fed for the day.

4.2.3 Analysis Metrics

The metrics used for this analysis are probability of unit detection for each electrode, average number of units per electrode, and median SNR, all as a function of impedance. The probability of unit detection compiles all electrodes within binned impedance ranges and calculates the ratio of electrodes with at least one unit to the total number of electrodes. The average number of units similarly bins electrodes by impedance and calculates the average number of units per electrode, as many electrodes recorded activity from multiple single units. Lastly, the median SNR of all units was calculated by compiled SNR measurements for all electrodes within a certain impedance range. Only units classified as motor units, by methods discussed in chapters 2 and 3, are included in this impedance analysis.

4.3 RESULTS AND DISCUSSION

This study was undertaken to test for any influences of electrode impedance upon signal quality in microelectrode arrays implanted chronically in the ventral roots. This was done by measuring impedances weekly and analyzing signal quality by a number of metrics involving calculations of SNR and unit yield of recording sites. The exposed tip lengths (site size) were also compared, seeking to improve electrode design by clearly specifying a site size that ensures high SNR along with high yield.

All impedances are in kilo-Ohms (kΩ) and binned for every 100 kΩ (0-100, 100-200, etc.) to 1000 kΩ for all data presented. Electrodes with an impedance greater than 1000 kΩ rarely recorded units. All impedances presented here were recorded at 1 kHz.

A 1-way ANOVA test was performed to compare the means of all groups for each set of data presented. If the p-value from the ANOVA was less than 0.05, the null hypothesis (that the means of all groups was equal) was rejected and post-hoc analysis was performed using Tukey's least significant difference procedure, a t-test that is applicable if the 1-way ANOVA shows a significant difference.

4.3.1 Impedances over time

Figure 4.1 shows an example of chronic impedance measurements of both arrays, denoted as L6 and L7, in cat W over the lifetime of the implants. Out of 32 electrodes, there were 8 electrodes of each site size; cat W was in group 1 and had site sizes of 25, 50, 100, and 150 μm. The line plot shows the median impedance of the 8 electrodes of a particular site size and the error bars express the upper and lower quantiles of the data. The numbers above the plot represent the number of electrodes that had high impedances (> 2000 kΩ) and were deemed to be broken; the neural recordings on these electrodes were virtually non-existent or highly noisy, and they were not included in the chronic impedance data below. The impedances measured before the implantation are also shown.

The electrical impedances, in general, were inversely correlated with site size, as expected. A smaller recording site surface area would lead to high resistance and impedance, as seen here. The impedances increased after implantation but remain stable while implanted, aside from electrode shanks that may have broken and escalated in impedance to values greater than 2000 kΩ. The variance of the electrodes also tended to increase, as the error bars overlap between site sizes as the implant time increased.

While the actual values varied, the trend of impedances over time remained the same for all cats, with site size inversely correlated to electrical impedance and relatively stable impedances throughout after an initial increase upon implantation. The lifetimes of the cats varied, as discussed in the previous chapter, based on the quality of the implant and any immune reactions.

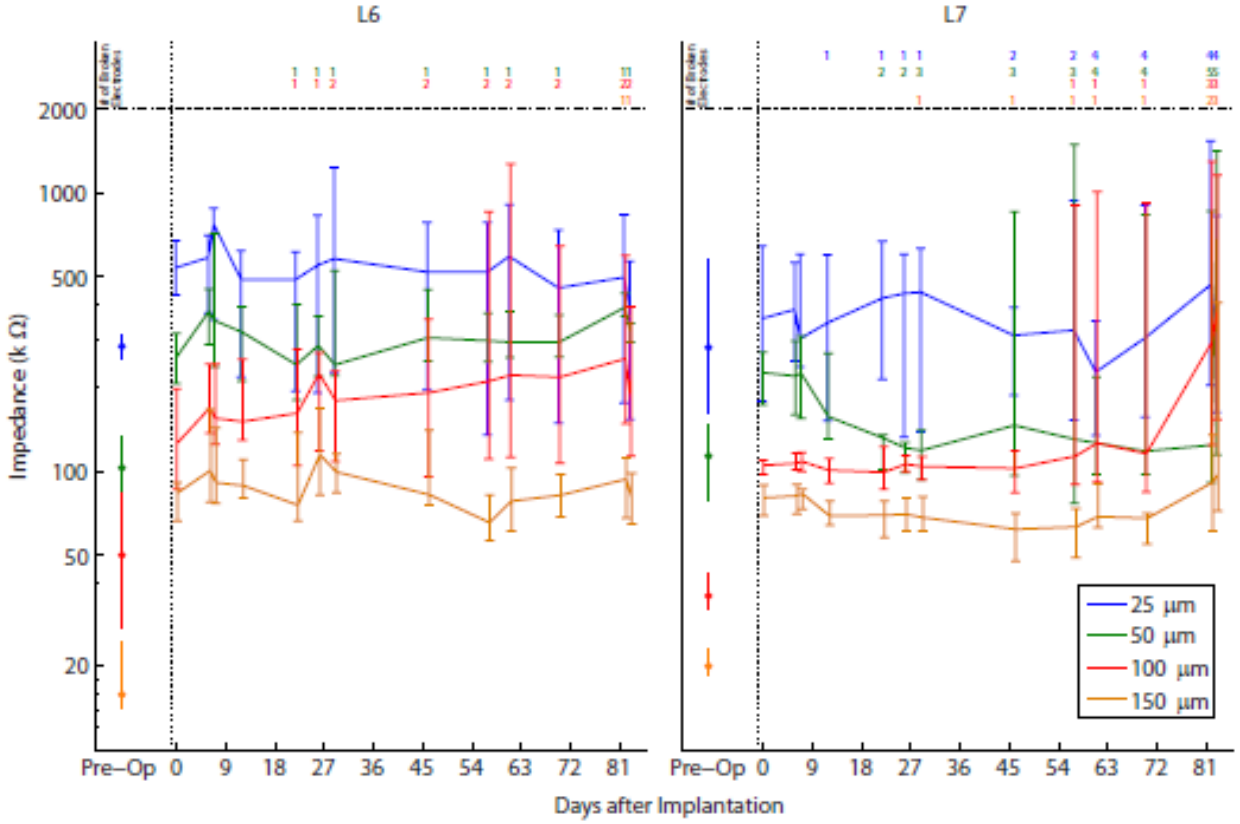

Figure 4.1. Impedances over time separated by site size. Shown is an example of 1 kHz impedance recordings over time in cat W for arrays in both L6 and L7 (from left to right). The line plots represent the median impedance for all electrodes of a particular site size, shown in the legend, while the error bars show the upper and lower quantiles of the data. The numbers above represent the number of "broken" electrodes with impedance greater than 2000 kΩ; these are not included in the line plots.

4.3.2 All signal quality metrics for all recording electrodes

The recordings of the electrodes (all site sizes) were compiled to calculate the signal quality metrics shown in Figure 4.2. Given an impedance, the probability of detecting a unit is shown in 4.2A, with the average number of units detected (not including channels without units) in 4.2B. Finally, 4.2C shows the median SNR of those detected units.

The probability of unit detection remained relatively uniform over all electrodes, though there is increased probability within the range of 200 to 500 kΩ and drops lower with increased impedance. The average number of units results reflect similar findings, though the number of units detected is higher for impedances below 800 kΩ. Impedances greater than 800 detected significantly lower numbers of units. The median SNR also remains between 2 and 5 for all impedances, while SNR values less than 1.2 were not considered. If 0-800 kΩ can be considered a functioning impedance range based on the previous two plots, the high end of this range detected units with significantly higher SNR.

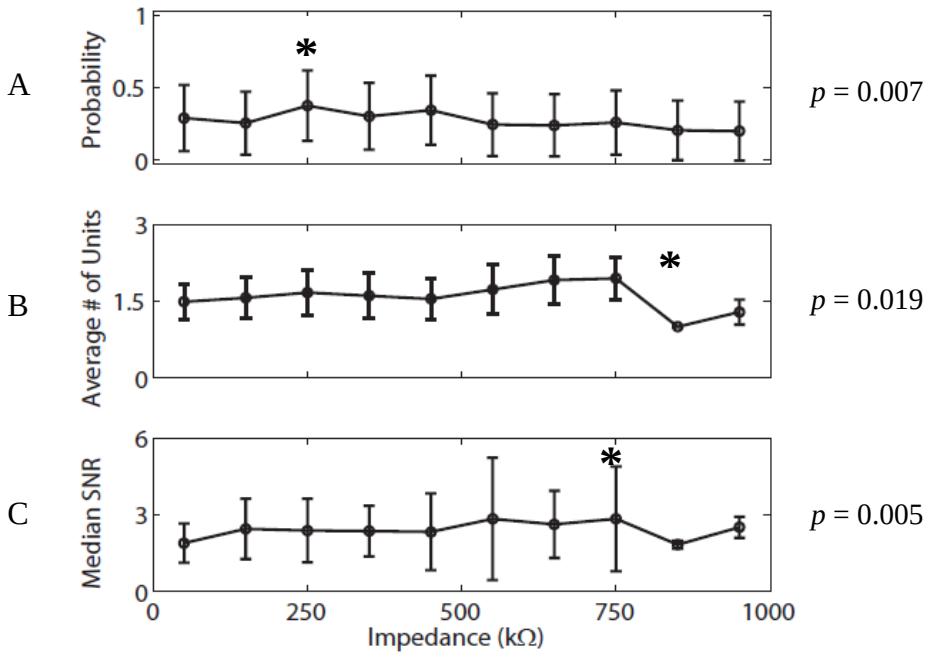

Figure 4.2. All signal quality metrics for all recording electrodes. From top to bottom, the probability of unit detection, the average number of units detected, and the median SNR of detected units as a function of impedance are shown. All data is binned for every 100 kΩ to 1000 kΩ. The p-values, results of 1-way ANOVA, are shown to the right. Results of post-hoc analysis, by Tukey's least significance difference procedure, are shown by asterisks noting groups significantly different from at least half of the other groups.

4.3.3 Probability of unit detection, separated by site size

The effects of impedance on signal quality are observed more clearly after separating all recording electrodes by site size. Figure 4.3 shows the probability of unit detection for each of the 8 site sizes as a function of impedances. In general, as discussed in section 4.3.1, impedances are higher for smaller sizes. The peaks in probability of unit detection tend to shift to lower impedances with increased site size. While there were no clear trends with all site sizes compiled, it can be seen here that each site size has its own ideal impedance range, which also

shifts to lower impedances for larger exposures. This is most clearly noticeable for site sizes 40, 80, and 160 μm; the peak of unit detection occurs in ranges of 700-800, 400-500, and 200-300 kΩ, respectively.

4.3.4 Average number of units, separated by site size

The average number of units, the second metric of signal quality, is shown in Figure 4.4 as a function of impedance and separated by site size. All site sizes recorded units within ranges that are shown in the plots for probability of unit detection. The highest number of units was also recorded at the peaks of probability of unit detection in Figure 4.3. Most channels recorded 1 or 2 units, leading an average of about 1.5 across all site sizes, while the average number of units increased beyond this, notably and significantly within the ideal impedance ranges for 40 and 160 μm, averaging almost 2 to 3 units per channel. The ideal impedance ranges for more units is very similar to that for unit detection and shifted to lower impedances for large exposures.

4.3.5 Median SNR, separated by site size

The final metric of signal quality, median SNR, is shown as a function of impedance and separated by site size in Figure 4.5. Most units recorded had an SNR value within 2 and 5. All site sizes recorded units of similar SNR and had few cases of well isolated units with a higher SNR. It can be seen that units of higher SNR were recorded at higher ends of the ideal impedance ranges for unit detection for each site size. There are neither significantly deficient nor adept electrode site sizes in terms of recording units with high SNR.

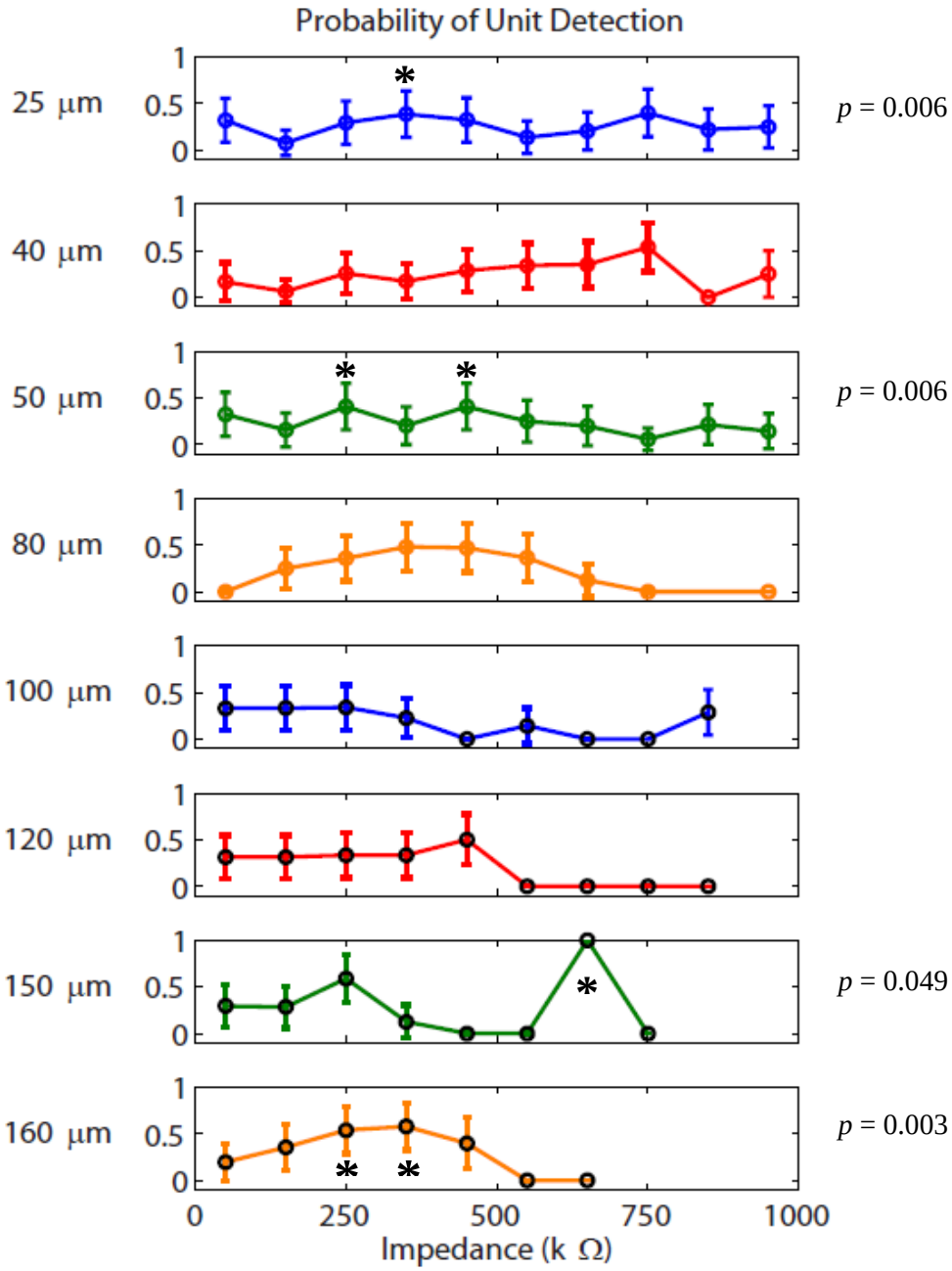

Figure 4.3. Probability of unit detection separated by site size. Shown as a function of impedance and listed by site size in increasing order. All data is binned for every 100 kΩ to 1000 kΩ. The significant p-values, results of 1-way ANOVA, are shown to the right. Results of post-hoc analysis, by Tukey's least significance difference procedure, are shown by asterisks noting groups significantly different from at least half of the other groups.

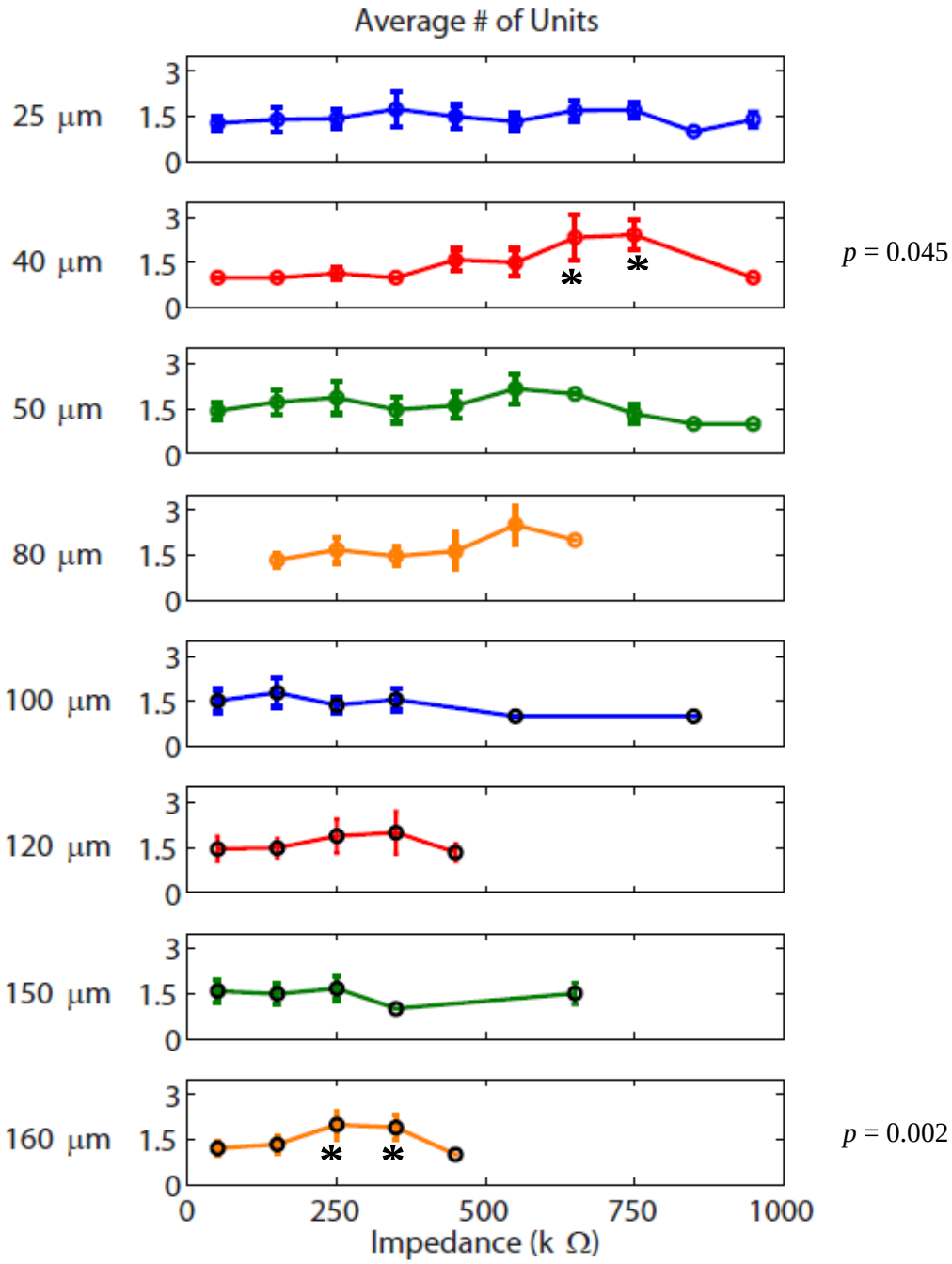

Figure 4.4. Average number of units separated by site size. Shown as a function of impedance and listed by site size in increasing order. All data is binned for every 100 k kΩ to 1000 kΩ. The significant p-values, results of 1-way ANOVA, are shown to the right. Results of post-hoc analysis, by Tukey's least significance difference procedure, are shown by asterisks noting groups significantly different from at least half of the other groups.

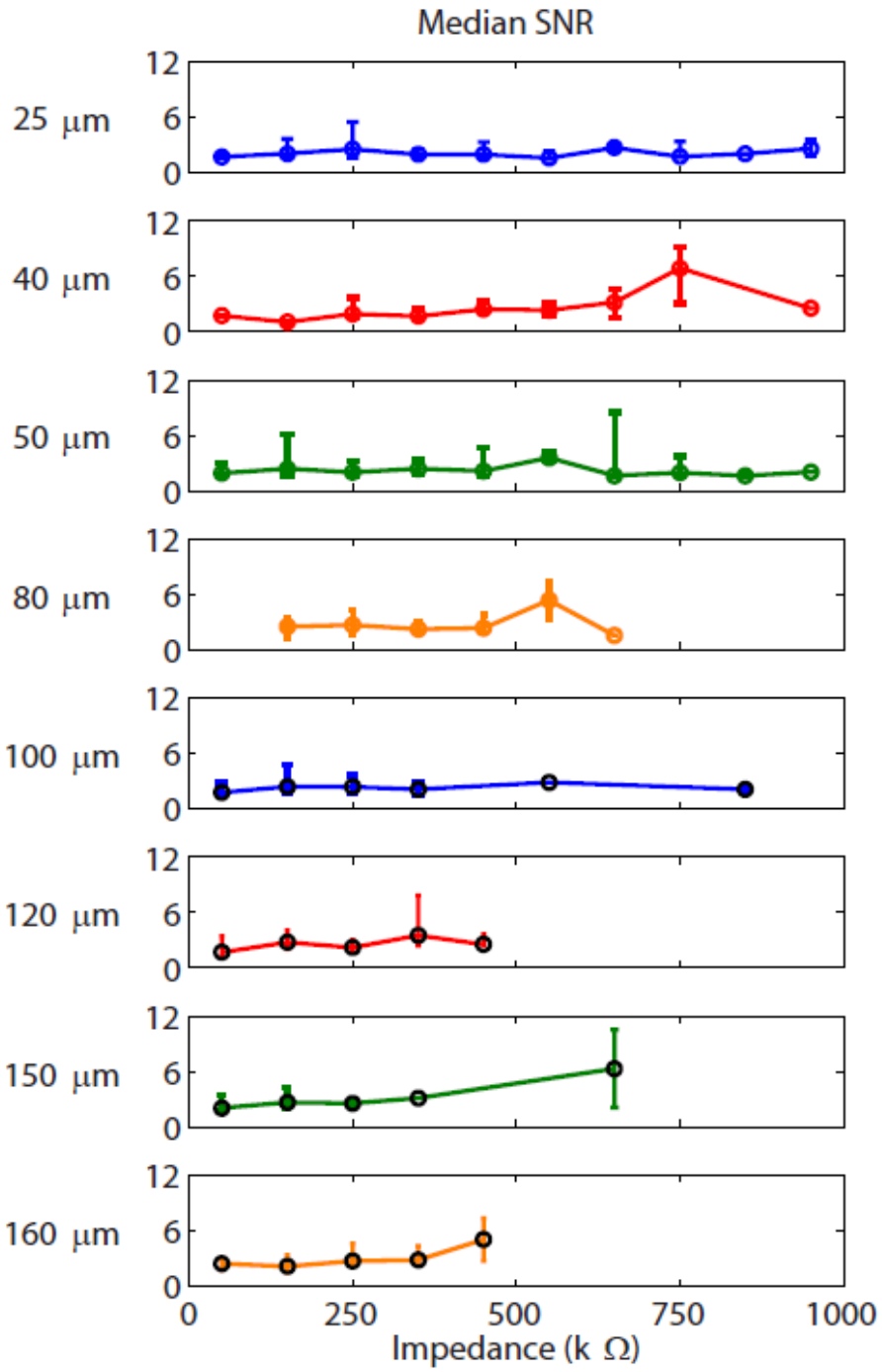

Figure 4.5. Median SNR separated by site size. Shown as a function of impedance and listed by site size in increasing order. All data is binned for every 100 kΩ to 1000 kΩ.

4.3.6 All signal quality metrics for electrodes with site size of 160 μm

By extracting the signal quality measurements of a particular site size, the effect of impedances can be unmasked. Figure 4.6 shows the signal quality metrics as a function of impedance for only the site size of 160 μm. The ideal range of impedance for unit detection is quite clear, peaking between 200 and 400 kΩ. Figure 4.6B, showing the average number of units, is shaped similarly, with significant peaks at impedances between 200 and 400 kΩ. There is a noticeable peak in Figure 4.6C; units with a higher SNR were measured at higher impedance within the range 500 to 600 kΩ. While increased impedance, in general, does not lead to higher SNR values, the high end of an ideal impedance range for a particular site size can bring about more isolated signals and increased SNR.

4.3.7 Comparison to Prasad et al.

Because of a similar theme, measuring electrical impedance of electrodes for neural recording, it is useful to view results in comparison with that of Prasad et al. [65]. The Prasad et al. study, as discussed in section 2.2.1, presented chronic impedance measurements and discussed relationships with the probability of unit detection. In that study, the ideal impedance range for unit detection was between 50 and 150 kΩ, much lower than the results presented in this chapter. This is likely because the electrodes used in that investigation had a recording site area of 7854 μm^2, which had average impedances in the range of 50 to 200 kΩ. The impedances presented in this chapter, in general, are higher, which can be attributed to smaller exposure site areas (Table 3.1); the largest exposures had an area of approximately 5419 μm^2. It may be useful to also note

that tungsten microwires were used by Prasad et al., while the studies here used platinum-iridium floating microelectrode arrays.

The Prasad et al. investigation did not report SNR trends nor any effect of site size or recording site surface area and their relationship with electrical impedance measurement.

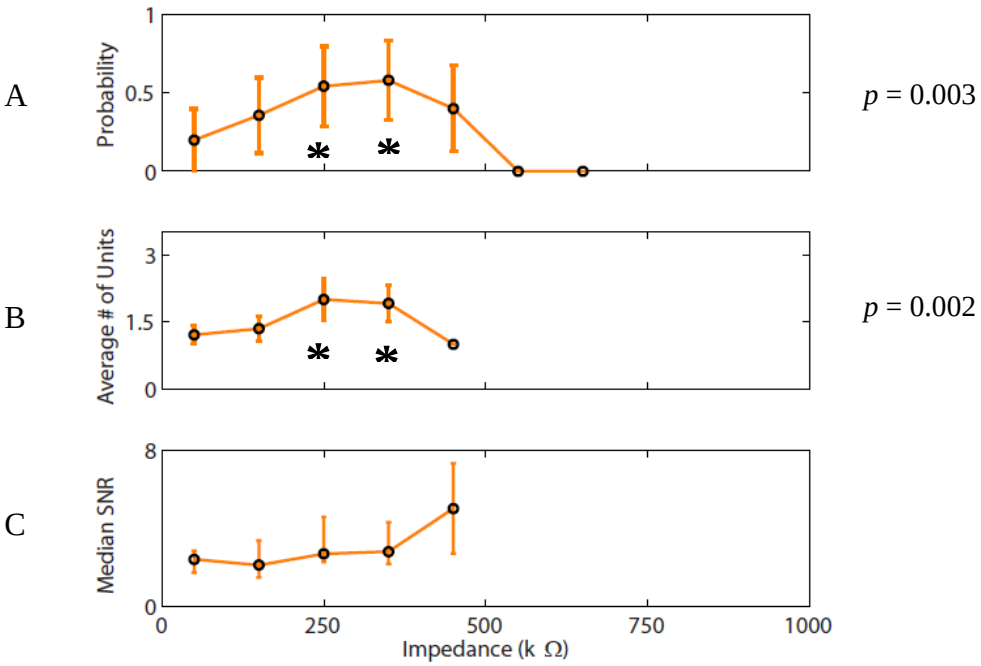

Figure 4.6. All signal quality for 160 µm electrodes. From top to bottom, the probability of unit detection, the average number of units detected, and the median SNR of detected units as a function of impedance are shown. All data is binned for every 100 kΩ to 1000 kΩ. The significant p-values, results of 1-way ANOVA, are shown to the right. Results of post-hoc analysis, by Tukey's least significance difference procedure, are shown by asterisks noting groups significantly different from at least half of the other groups.

4.4 FUTURE WORK AND CONCLUSIONS

Future plans for this work include increased sampling of impedance measurements, as well as applying signal quality metrics to electrodes implanted in other targets, including the dorsal root ganglia, peripheral nerves, and cortical areas of the brain. A future goal is to fit impedance data to produce a statistical model that can predict the behavior (possibility of unit detection or electrode failure) of an implanted electrode, given its site size and impedance measurement.

Only impedance measurements at 1k Hz were presented here. Measurements at all other frequencies can be applied towards the adaptation of an equivalent circuit model to better interpret impedance recordings. The magnitude and phase components of the impedance can be used to calculate the real and imaginary components of the complex impedance; plotting the imaginary versus real components produces a Nyquist plot, which can be fit after testing a number of complex circuit models. The examples of equivalent circuits in Figure 2.3 are the building blocks for these models. The behavior of electrical impedance at different frequencies can be attributed to a variety of possible responses and elements of the electrode-tissue interface.

This study has examined chronic electrical impedances of floating microelectrode arrays implanted into the spinal roots of cats. The signal quality of neural recordings was analyzed in terms of measured impedances. Three metrics, probability of unit detection, the average number of units, and median SNR, were presented as functions of impedance. Ideal impedance ranges were found after separating these metrics by electrode site size. SNR and total unit yield were used for further site size analysis, omitting impedances. This investigation can be applied for electrode design improvements by stating site size specification based on impedance, unit yield, and SNR requirements for electrodes implanted in the spinal cord, brain, or peripheral targets.

5.0 CONCLUSION

5.1 SUMMARY OF RESULTS

This thesis describes a novel approach to implanting floating microelectrode arrays into the ventral roots, a unique electrophysiological target that has not been explored extensively. The unique anatomy at the spinal roots, where the motor and sensory neural signals are segregated in tissue by the division of dorsal and ventral roots, makes them a potential area of study for a reliable peripheral interface.

Chapter 1 introduced the current state of neural engineering and neural prosthetics, while considering the possibility of a reliable peripheral interface that incorporates signals from the spinal roots.

Chapter 2 described the background of methods used in this thesis, particularly a recently developed algorithm used to separate motor and sensory signals by a number of heuristic metrics. The measurements used to quantify ventral root recordings were examined. This chapter also included a report on electrical impedance and reviewed a notable study that related impedances to signal quality of chronic impedance measurements.

Chapter 3 provided the methods of implantation and experimentation used for neural recordings and described the results of analysis by reporting signal-to-noise ratios and single unit

yield for all implanted animals and arrays. Ventral root recordings were shown to be successful through 12 weeks post-operation, with a relatively high number of units for up to 6 weeks and a median of SNR values greater than 2 throughout the life of the implants. By including future work that can identify target muscles from spike-triggered averaging of EMG recordings, it may possible to decode ventral root recordings to control a motor neuroprosthetic device from a peripheral interface.

Chapter 4 discussed methods of measuring electrical impedances on every implanted electrode and presented results of chronic measurements. The electrode tip length specifications, or site sizes, were also discussed. Signal quality was analyzed as a function of impedance as well as site size, and it was found that each site size has its own ideal impedance range that increases the probability of unit detection. The high end of this impedance range also tended towards units of greater SNR. The impedance ranges for isolating a number of single units on a single channel trended similarly with those for higher probability of unit detection. It was found that the smallest site sizes (< 50 μm) recorded significantly fewer units than the larger site sizes, which recorded similar numbers. All site sizes, however, recorded units with similar SNR values. The results from this chapter can be used to improve electrode design and electrode site size specifications for future applications.

5.2 CONCLUDING REMARKS

Although widespread clinical and commercial translation of products in neural engineering has been limited, much progress has been achieved in all aspects of the field of neural prosthetics. In the field of brain-computer interfaces, there have been huge strides in every element, from

improved neural ensemble decoding and translation to increasingly complex robotic devices and computer tasks. There remains some critical work to be done to reduce invasiveness, as well as improve longevity of usefulness. While another electrophysiological target may not be the answer, the research community has the knowledge and means to examine every potential way to move forward. As for the answer to chronic reliability, until a method is developed to effectively extend the functional lifetime of these implants, commercial and clinical applications will remain unattainable. The measures of electrical impedance, while only a slightly predictive measure, can be used as a tool towards reaching these goals, as well as a method of estimating electrode viability and sustainability.

Interfaces that include the brain, spinal cord, or spinal roots have the potential to significantly improve the wellbeing and lifestyle of millions of disabled patients around the world. Finding solutions for these individuals remains a very relevant field of study, as demonstrated by the growth of neural engineering studies. It is likely that the next few decades may allow the birth of the next generation of neural prosthetics. This possibility will require the combination of multi-disciplinary research and expansive knowledge in electrophysiological targets and the human brain.

BIBLIOGRAPHY

1. Schwartz AB, Cui XT, Weber DJ, Moran DW (2006) Brain-Controlled Interfaces: Movement Restoration with Neural Prosthetic. Neuron 52(1):205-220

2. Hochberg LR, Serruya MD, Frieghs GM, Mukand JA, Saleh M, Caplan AH, Branner A, Chen D, Penn RD, Donoghue JP (2006) Neuronal ensemble control of prosthetic devices by a human with tetraplegia. Nature 442(7099):164-71

3. Schultz AE, Kuiken TA. (2011) Neural Interfaces for Control of Upper Limb Protheses: The State of the Art and Future Possibilities. PM&R 3:55-67

4. Ziegler-Graham K, MacKenzie EJ, Ephraim PL, Travison TG, Brookmeyer R (2008) Estimating the prevalence of limb loss in the United States: 2005 to 2050. Arch Phys Med Rehabil 89(3):422-9

5. One Degree of Separation: Paralysis and Spinal Cord Injury in the United States (2009) Christopher & Dana Reeve Foundation.

6. Schwartz AB (2004) Cortical Neural Prosthetic. Annu Rev Neurosci 27:487-507

7. Deep Brain Stimulation for Movement Disorders (2013) Medtronic.

8. Cochlear Implants (2011). NIH Publication 11-4798

9. Medicare Designates Argus II Retinal Prosthesis System as New Technology and Provides Payment (2013) Second Sight.

10. Hjorth B (1970) EEG analysis based on time domain properties. Electroenceph Clin Neurophys 76:197-204

11. Quesney LF, Gloor P (1985) Localization of epileptic foci. Electroenceph Clin Neurophys 37: 165-200

12. Cuffin BN (1996) EEG Localization Accuracy Improvements Using Realistically Shaped Head Models. IEEE Trans on Biomed Eng 43(3):299-303

13. Kupfer DJ, Foster FG, Coble P, McPartland RJ, Ulrich RF (1978) The Application of EEG Sleep for the Differential Diagnosis of Affective Disorders. Am J Psychiatry 135(1):69-74

14. Kupfer DJ, Thase ME (1983) The use of the sleep laboratory in the diagnosis of affective disorders. Psychiatric Clinics of North America 6(1):3-25

15. Fenton, GW (1986) The EEG, epilepsy, and psychiatry. *What is Epilepsy* 139-160

16. Smith EJM (2005) EEG in the diagnosis, classification, and management of patients with epilepsy. J Neural Neurosurg Psychiatry 76:ii2-ii7

17. Cohen D, Cuffin BN, Yunokuchi K, Maniewski R, Purcell C, Cosgrove GR, Ives J, Kennedy JG, Schomer DL (2004) Annals of Neurology 28(6):811-817

18. Malmivuo J (2012) Comparison of the properties of EEG and MEG in detecting the electric activity of the brain. Brain Topogr 25(1):1-19

19. Hämäläinen M, Hari R, Ilmoniemi J, Knuutila J, Lounasmaa OV (1993) Magnetoencephalography – theory, instrumentation, and application to noninvasive studies of the working human brain. Rev Mod Phys 65:413-497

20. Foldes ST, Wang W, Collinger J, Li X, Zhang J, Sudre G, Bagic A, Weber DJ (2011) Accessing and Processing MEG Signals in Real-Time: Emerging Applications and Enabling Technologies. *Magnetoencephalography* 211:234

21. Colon AJ, Ossenblock P, Nieuwenhuis L, Stam KJ, Boon P (2009) Use of routine MEG in the primary diagnostic process of epilepsy. J Clin Neurophysiol 26(5):326-32

22. Halgren E, Raij T, Marinkovic K, Jousmäki V, Hari R (2000) Cerebral Cortex 10(1):69-81

23. Alho K, Kujala T, Paavilainen P, Summala H, Näätänen R (1993) Auditory processing in visual brain areas of the early blind: Evidence from even-related potentials. Electroenceph Clin Neurophys 86:418-427

24. Salmelin R. Clinical neurophysiology of language: The MEG approach (2007) Clin Neurophyc 118(2):237-254

25. Asano E, Juhasz C, Shah A, Muzik O, Chugani DC, Shah J, Sood S, Chugani HT (2005) Epilepsia 46(7):1086-1097

26. Micera S (2010) Control of Hand Prostheses Using Peripheral Information. IEE Rev in Biomed Eng 3:48-68

27. Stieglitz T, Schuettler M, Koch KP (2005) Implantable Biomedical Microsystems for Neural Prostheses. IEEE Eng in Med Biol 24(5):58-65

28. Tyler DJ, Durand DM (2002) Functionally selective peripheral nerve stimulation with a flat interface nerve electrode. IEE Trans Neural Syst Rehabili Eng 10(4)294-303

29. Dhillon GS, Lawrence SM, Hutchinson DT, Horch KW (2004) Residual function in peripheral nerve stumps of amputees: implications for neural control of artificial limbs. J Hand Surg Am 29(4):605-18

30. Farina D, Merletti R, Enoka RM (2004) The extraction of neural strategies from the surface EMG. J Appl Physiol 96(4):1486-95

31. Schalk G, McFarland DJ, Hinterberger T, Birbaumer N, Wolpaw JR (2004) BCI2000: a general-purpose brain-computer interface (BCI) system. IEEE Trans on Biomed Eng 51(6):1034-1043

32. Wolpaw JR, McFarland DJ, Neat GW, Forneris CA (1991) An EEG-based brain-computer interface for cursor control. Electroenceph Clin Neurophys 78(3):252-259

33. Wolpaw JR, Birbaumer N, McFarland DJ, Pfurtscheller G, Vaughan TM (2002). Clin Neurophys 113(6):767-791

34. Foldes ST (2010) Control of a Virtual Neuroprosthesis-Arm with Noninvasive Field Potentials. Electronic Thesis or Dissertation, Case Western University.

35. Foldes ST, Vinjamuri RK, Wang W, Weber DJ, Collinger JL (2011) Stability of MEG for Real-time Neurofeedback. Conf Proc IEEE Eng Med Biol Soc: 5778-5781

36. Wang W, Collinger JL, Perez MA, Tyler-Kabara EC, Cohen LG, Birbaumer N, Brose SW, Schwartz AB, Boninger ML, Weber DJ (2010) Neural Interface Technology for Rehabilitation: Exploiting and Promoting Neuroplasticity. Phys Med Rehab Clin N Am 21(1):157-178

37. Velliste M, Perel S, Spalding MC, Whitford AS, Schwartz AB (2008) Cortical control of a prosthetic arm for self-feeding. Nature 453:1098-1101

38. Lebedev MA, Nicolelis MA (2006) Brain-machine interfaces: past, present, and future. Trends Neurosci 29(9):536-46

39. Collinger JL, Wodlinger B, Downey JE, Wang W, Tyler-Kabara EC, Weber DJ, McMorland AJC, Velliste M, Boninger ML, Schwartz AB (2013) High-performance neuroprosthetic control by an individual with tetraplegia. The Lancet 381(9866):557-564

40. Wang W, Collinger JL, Degenhart AD, Tyler-Kabara EC, Schwartz AB, Moran DW, Weber DJ, Wodlinger B, Vinjamuri RK, Ashmore RC, Kelly JW, Boninger ML (2013) An Electrocorticographic Brain Interface in an Individual with Tetraplegia. PLoS ONE 8(2): e55344

41. Rossini PM, Micera S, Benvenuta A, Carpaneto J, Cavallo G, Citi L, Cipriani C, Denaro L, Denaro V, di Pino G, Ferrari F, Guglielmelli E, Hoffman KP, Raspopovic S, Rigosa J, Rossini L, Tombini M, Dario P (2010). Clin Neurophys 121(5):777-783

42. Korbinski AE, Bolkovitin SV, Voskoboinikova LM (1960) Problems of Bioelectric Control. Conf Proc Intl Congress of Auto and Remote Control 2:619-629

43. Baughn B (2004) The Myoelectric Myth. International Child Amputee Network.

44. Kuiken TA, Li G, Lock BA, Lipschutz RD, Miller LA, Stubblefield KA, Englehart KB (2009) Targeted Muscle Reinnervation for Real-time Myoelectric Control of Multifunction Artifical Arms. JAMA 301(6):619-628

45. Kuiken TA, Childress DS, Rymer WZ (1995) The hyper-reinnervation of rat skeletal muscle. Brain Res 676(1):113-23

46. Kuiken TA, Dumanian GA, Lipschutz RD, Miller LA, Stubblefield KA (2004) The use of targeted muscle reinnervation for improved myoelectric prosthesis control in a bilateral shoulder disarticulation amputee. Pros and Orth Intl 28(3):245-253

47. Minimally Invasive Surgery MIS (2009) American Association of Neurological Surgeons.

48. Hoffer JA, Loeb GE, Marks WB, O'Donovan MJ, Pratt CA, Sugano N (1987) Cat hindlimb motoneurons during locomotion I: Destination, axonal conduction velocity, and recruitment threshold. J Neurophysiol 57:510-529

49. Hoffer JA, Sugano N, Loeb GE, Marks WB, O'Donovan MJ, Pratt CA (1987) Cat hindlimb motoneurons during locomotion II: Normal activity patterns. J Neurophysiol 57:530-553

50. Hoffer JA, Loeb GE, Sugano N, Marks WB, O'Donovan MJ, Pratt CA (1987) Cat hindlimb motoneurons during locomotion III: Functional segregation in Sartorius 57:554-562

51. Loeb GE, Marks WB, Hoffer JA (1987) Cat hindlimb motorneurons during locomotion IV: Participation in cutaneous reflexes 57:563-573

52. Merrill DR, Bikson M, Jeffreys JGR (2005) Electrical stimulation of excitable tissue: design of efficacious and safe protocols. J Neurosci Methods 141:171-198

53. Cogan SF (2008) Neural Stimulation and Recording Electrodes. Annu Rev Biomed Eng 10:275-309

54. Marblestone AH, Zamft BM, Maguire YG, Shapiro MG, Cybulski TR, Glaser JI, Amodei D, Stranges PB, Kalhor R, Dalrymple DA, Seo D, Alon E, Maharbiz MM, Carmena JM, Rabaey JM, Boyden ES, Church GM, Kording KP (2013) Physical Principles for Scalable Neural Recording. Draft for submission.

55. Williams JC, Rennaker RL, Kipke DR (1999) Long-term neural recording characteristics of wire microelectrode arrays implanted in cerebral cortex. Brain Res Prot 4(3):303-313

56. Nicolelis MA, Lebedev MA (2009) Principles of neural ensemble physiology underlying the operation of brain-machine interfaces. Nature Rev Neurosci 10:530-540

57. Simeral JD, Kim SP, Black MJ, Donoghue JP, Hochberg LR (2011) Neural control of cursor trajectory and click by human with tetraplegia 1000 days after implant of an intracortical microelectrode array. J Neural Eng 8(2):025027

58. Chestek CA, Gilja V, Nuyujukian P, Foster JD, Fan JM, Kaufman MT, Churchland MM, Riviera-Alvidrez Z, Cunninghamg JP, Ryu SI, Shenoy KV (2011) Long-term stability of neural prosthetic control signals from silicon cortical arrays in rhesus macaque motor cortex. J Neural Eng 8(4):045005

59. Collinger JL, Kryger MA, Barbara R, Betler T, Bowsher K, Brown EHP, Clanton ST, Degenhart AD, Foldes ST, Gaunt RA, Gyulai FE, Harchick EA, Harrington D, Helder JB, Hemmes T, Johannes MS, Katyal KD, Ling GSF, McMorland AJC, Palko K, Para MP, Scheuermann J, Schwartz AB, Skidmore ER, Solzbacher F, Srikameswaran AV, Swanson DP, Swetz S, Tyler-Kabara EC, Velliste M, Wang W, Weber DJ, Wodlinger B, Boninger ML (2013) Collaborative Approach in the Development of High Performance Brain-Computer Interfaces for a Neuroprosthetic Arm: Translation from Animals Models to Human Control. Clin and Trans Sci 0(0):1-8

60. Cutsem MV, Duchateau J, Hainaut K (1998) Changes in single motor unit behavior contribute to the increase in contraction speed after dynamic training in humans. J Physiol 513:295-305

61. Christou EA (2010) Interspike Interval. *Encylopedia of Movement Disorders, Volume 1* 81-83

62. Williams JC, Hippensteel JA, Dilgen J, Shain W, Kipke DR (2007) Complex impedance spectroscopy for monitoring tissue responses to inserted neural implants. J Neural Eng 4(4):410-23

63. Ward MP, Rajdev P, Ellison C, Irazoqui PP (2009) Toward a comparison of microelectrodes for acute and chronic recordings. Brain Res 1282:183-200

64. Frampton JP, Hynd MR, Schuler ML, Shain W (2010) Effects of glial cells on electrode impedance recorded from neural prosthetic devices in vitro. Ann Biomed Eng 38(3):1031-47

65. Prasad A, Sanchez JCC (2012) Quantifying long-term microelectrode array functionality using chronic *in vivo* impedance testing. J Neural Eng 9:026028

66. Karp FB, Bernotski NA, Valdes TI, Böhringer KF, Ratner BD (2008) Foreign Body Response Investigated with an Implanted Biosensory by *in situ* Electrical Impedance Spectroscopy. IEEE Sensors J 8(1):104-112

67. Ethylene Oxide (EtO) Sterilization Process (2013) Eurotherm.

68. User Instructions for Floating Microelectrode Array (FMA) (2013). MicroProbes for Life Science.